

IsoCLIP: Decomposing CLIP Projectors for Efficient Intra-modal Alignment

Simone Magistri^{1*} Dipam Goswami^{2,3} Marco Mistretta¹ Bartłomiej Twardowski^{2,3,4}
 Joost van de Weijer^{2,3} Andrew D. Bagdanov¹

¹ Media Integration and Communication Center (MICC), University of Florence, Italy

²Department of Computer Science, Universitat Autònoma de Barcelona, Spain

³Computer Vision Center, Barcelona, Spain ⁴IDEAS Research Institute, Warsaw, Poland

{simone.magistri, marco.mistretta, andrew.bagdanov}@unifi.it

{dgoswami, btwardowski, joost}@cvc.uab.cat

Abstract

Vision-Language Models like CLIP are extensively used for inter-modal tasks which involve both visual and text modalities. However, when the individual modality encoders are applied to inherently intra-modal tasks like image-to-image retrieval, their performance suffers from the intra-modal misalignment. In this paper we study intra-modal misalignment in CLIP with a focus on the role of the projectors that map pre-projection image and text embeddings into the shared embedding space. By analyzing the form of the cosine similarity applied to projected features, and its interaction with the contrastive CLIP loss, we show that there is an inter-modal operator responsible for aligning the two modalities during training, and a second, intra-modal operator that only enforces intra-modal normalization but does nothing to promote intra-modal alignment. Via spectral analysis of the inter-modal operator, we identify an approximately isotropic subspace in which the two modalities are well-aligned, as well as anisotropic directions specific to each modality. We demonstrate that this aligned subspace can be directly obtained from the projector weights and that removing the anisotropic directions improves intra-modal alignment. Our experiments on intra-modal retrieval and classification benchmarks show that our training-free method reduces intra-modal misalignment, greatly lowers latency, and outperforms existing approaches across multiple pre-trained CLIP-like models. The code is publicly available at: <https://github.com/simomagi/IsoCLIP>.

1. Introduction

Pre-trained Vision-Language Models (VLMs) like CLIP [34] are widely used for applications ranging

from image and text retrieval [2, 36], to open-vocabulary segmentation [14, 53], generalized category discovery [5, 46] and visual question answering [30, 40]. CLIP is trained contrastively on a massive dataset of image-text pairs to align image and text representations from the vision and text encoders by projecting them in a shared embedding space. This joint embedding space has fostered a broad range of inter-modal applications leveraging the power of the semantically-aligned image and text encoders.

While primarily designed for inter-modal tasks like zero-shot object recognition, CLIP has been applied to intra-modal tasks due to its rich pre-trained image and text encoders. Several works use the CLIP image encoder for image-to-image retrieval [18, 25, 27, 28, 37], sketch-based image retrieval [36], and the CLIP text encoder for text-to-text retrieval [25, 50]. Furthermore, CLIP image encoders have also been extensively used for computing intra-modal image-to-image similarities for tasks like image classification [12, 43, 49, 56] and text-to-image generation [10, 35]. While it is desirable to have a multi-modal model which can also be used for intra-modal tasks when required, the *intra-modal misalignment* inherent in CLIP – as pointed out in [25, 43, 52] – results in sub-optimal performance.

Intra-modal misalignment manifests because the contrastive training loss of CLIP maximizes only inter-modal cosine similarities while ignoring the intra-modal ones. Mistretta et al. [25] showed that approaching intra-modal tasks inter-modally can mitigate intra-modal misalignment. To demonstrate this, they introduced two *modality inversion* techniques – Optimization-based Text Inversion (OTI) and Optimization-based Visual Inversion (OVI) – which map a feature into the complementary modality.

In image-to-image retrieval, OTI converts a query image feature into a query text feature, which is then compared with the original gallery image features. Conversely, in text-to-text retrieval, OVI performs the opposite mapping, inverting a query text feature into an image feature. Although

*Corresponding author.

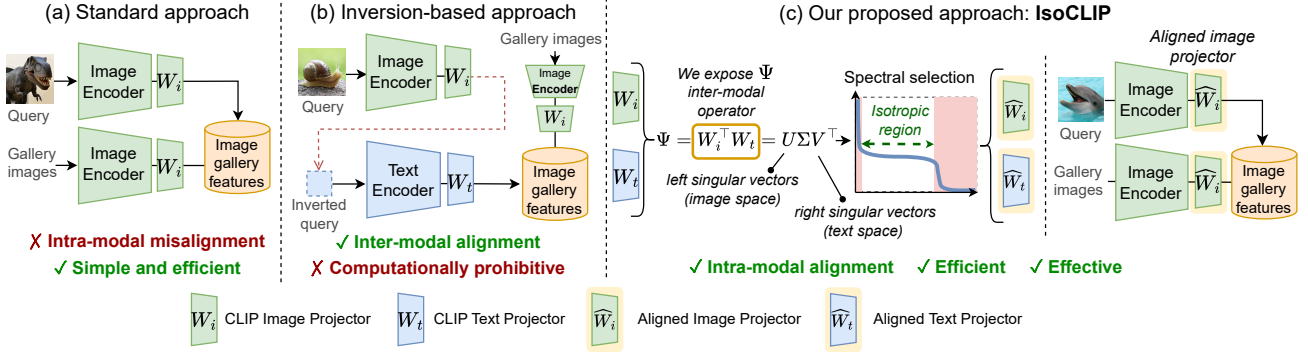


Figure 1. **Overview of intra-modal retrieval with CLIP.** (a) The standard approach simply compares the cosine similarities computed after applying projector W_i to query and gallery image embeddings, which is sub-optimal due to *intra-modal misalignment*. (b) To circumvent misalignment, inversion approaches [25] convert the query image embeddings to text embeddings by iteratively optimizing pseudo-tokens – an expensive operation that incurs high latency – and then computes inter-modal cosine similarities for retrieval. (c) We identify an inter-modal operator $\Psi = W_i^T W_t$ fundamental to CLIP cosine similarity computations. We propose IsoCLIP, which uses only an isotropic region of the spectrum of Ψ to align the projector weights along well-aligned directions between modalities. Then these *aligned* projectors are used to map the query and gallery embeddings. IsoCLIP exploits the properties of the CLIP projectors and does not add any latency to process while yielding more optimal intra-modal cosine similarities and significantly improved intra-modal performance.

they mitigate intra-modal misalignment, these techniques have significant limitations that hinder practical applicability. In particular, they require very many optimization steps and forward passes through the target modality encoder, and their performance is strongly dependent on the number of optimization steps which are difficult to determine a priori.

In this paper, we analyze the training loss of CLIP and its interaction with the projection heads used to project pre-projection feature embeddings into the aligned space. We show that there is an *inter-modal operator* hidden in the cosine similarity which connects the two pre-projection spaces and is responsible for aligning the image and text embeddings. We additionally show that, during backpropagation of the contrastive CLIP loss, an *intra-modal operator* is unveiled that guarantees normalization, but does nothing to promote intra-modal alignment. Via Singular Value Decomposition of the inter-modal operator, we identify an approximately isotropic subspace in which the two modalities are well-aligned and show how the two modalities behave in the different regions of the singular value spectra. Finally, we show (see Fig. 1) that restricting projectors to these identified isotropic directions yields more discriminative cosine similarities and significant improvement on intra-modal tasks like image-to-image retrieval, text-to-text retrieval. To summarize, our main contributions are:

- we analyze the role of CLIP projectors and dissect their interactions with the cosine similarity and contrastive loss, which reveals an inter-modal operator responsible for aligning modalities and an intra-modal operator responsible only for normalization;
- via spectral analysis of the inter-modal operator, we identify an approximately isotropic subspace in the middle band of the spectrum in which the modalities are well-

aligned and anisotropic bands at the top and bottom of the spectrum specific to each modality;

- we propose IsoCLIP, which enhances intra-modal alignment by retaining only well-aligned directions between text and images in the inter-modal operator while discarding anisotropic, modality-specific directions; and
- we experimentally demonstrate that IsoCLIP greatly reduces latency and consistently improves performance on a range of intra-modal tasks, including image-to-image retrieval, text-to-text retrieval across multiple datasets.

2. Related Work

In this section we review work from the recent literature most related to our contributions.

Vision-language models. Contrastively trained VLMs [3, 26, 34, 54] are widely used in many applications [14, 23, 30, 36, 53, 58]. Among these, CLIP is a prominent representative: it consists of an image and text encoder trained to output image and text embeddings that are aligned after projection into a shared embedding space. This embedding space can be considered a normalized hypersphere [21, 48].

Several recent studies [11, 20, 21, 25, 38, 39] have analyzed critical properties of VLMs which question our understanding of the shared multi-modal embedding space and its impact on inter-modal and intra-modal tasks. Liang et al. [21] showed that a *modality gap* exists between the image and text embeddings, even though they are trained to be aligned. This phenomenon was later attributed to information imbalance between image and text data [38].

In addition to inter-modal tasks, VLM encoders have also been repurposed as standalone encoders for tasks like image-to-image retrieval in which only the pre-trained or

finetuned image encoder is used for retrieval [18, 25, 27, 28, 37]. In this paper, we show that CLIP intra-modal similarities are sub-optimal and propose an effective, training-free approach to adapt pre-trained VLMs for intra-modal tasks.

Intra-modal misalignment. Recent works [25, 43, 52] investigated the *intra-modal misalignment* in the CLIP embedding space. Udandarao et al. [43] showed that the intra-modal image-to-image and text-to-text similarities have larger means and variances than inter-modal similarities. [25] proposed optimization-based methods (OTI and OVI) to invert the modality of the query by crossing the modality gap and performing *intra-modal tasks* using *inter-modal similarities*. These methods are expensive and require many optimization steps per query. In this work, we analyze the geometric properties of the CLIP projectors and how they combine, via cosine similarity, into a single *inter-modal operator*. We then exploit the spectral properties of the inter-modal operator to achieve better intra-modal alignment.

3. Inter- and Intra-modal Operators in CLIP

Prior work [25] has empirically shown that CLIP is suboptimal on intra-modal tasks like image-to-image or text-to-text retrieval when using a single modality encoder. This limitation has been linked to the *intra-modal misalignment*: CLIP’s contrastive loss aligns images and text, without promoting similarity within each modality.

In this section we expand on these findings by analyzing how the CLIP training loss reinforces inter-modal alignment. We show that this alignment can be formally understood from the structure of the CLIP projection heads.

3.1. The Role of the Projection Heads

We define the image and text encoders of CLIP as two mappings f_θ and g_ϕ , parametrized by weights θ and ϕ , respectively, which produce an image embedding $f_i = f_\theta(i) \in \mathbb{R}^{d_i}$ and a text embedding $g_t = g_\phi(t) \in \mathbb{R}^{d_t}$ for an image i and text t . Our goal is to characterize the inter-modal alignment and intra-modal misalignment between the image and text encoders of CLIP.

The cosine similarity under projection. CLIP maps image and text features f_i and g_t through two linear projector matrices $W_i \in \mathbb{R}^{d \times d_i}$ and $W_t \in \mathbb{R}^{d \times d_t}$, projecting them onto a shared d -dimensional embedding space: $F(f_i) = W_i f_i \in \mathbb{R}^d$ and $G(g_t) = W_t g_t \in \mathbb{R}^d$. The similarity between image-text pairs is computed as:

$$\text{sim}(f_i, g_t) = \frac{F(f_i)^\top G(g_t)}{\|F(f_i)\|_2 \|G(g_t)\|_2} = \frac{f_i^\top (W_i^\top W_t) g_t}{\|W_i f_i\|_2 \|W_t g_t\|_2}. \quad (1)$$

This shows that CLIP always relies on the *product between the two projectors* to compute cosine similarities. This product, which we define as

$$\Psi = W_i^\top W_t \in \mathbb{R}^{d_i \times d_t} \quad (2)$$

acts as an *inter-modal operator* $\Psi : \mathbb{R}^{d_t} \rightarrow \mathbb{R}^{d_i}$ that transforms the pre-projection text feature g_t into the corresponding image space. Its transpose Ψ^\top is the reverse mapping from images to texts. Thus, Ψ effectively serves as a bridge between two modalities. We will now show, via an analysis of the contrastive CLIP loss, that this operator is responsible for the *inter-modal* alignment between image and text encoders during training. This analysis will also unveil a hidden *intra-modal* operator that is the cause of *intra-modal misalignment* in CLIP.

Inter-modal and intra-modal operators. The symmetric contrastive loss of CLIP is defined as:

$$\mathcal{L}_{\text{CLIP}} = \frac{1}{2} (\mathcal{L}_{i \rightarrow t} + \mathcal{L}_{t \rightarrow i}), \quad (3)$$

where $\mathcal{L}_{i \rightarrow t}$ moves the embedding of each image i toward the corresponding *positive* paired text t , while pushing it away from all other texts in the mini-batch. The term $\mathcal{L}_{t \rightarrow i}$ performs the symmetric alignment in the opposite direction. We focus on $\mathcal{L}_{i \rightarrow t}$ for simplicity; it is defined as:

$$\mathcal{L}_{i \rightarrow t} = -\log \frac{\exp(\text{sim}(f_i, g_t)/\tau)}{\sum_{t'} \exp(\text{sim}(f_i, g_{t'})/\tau)} \quad (4)$$

where τ is the temperature, t is the *positive text* for image i , t' indexes both the positive and the negative texts in the mini-batch, and $\text{sim}(\cdot, \cdot)$ is the cosine similarity between the image and text features as defined in Eq. (1). To understand the effect of the inter-modal operator on the training dynamics of CLIP, we consider the gradient of the loss with respect to the pre-projection image feature f_i , focusing on the contribution of the pre-projection *positive* text embedding g_t :

$$\frac{\partial \mathcal{L}_{i \rightarrow t}}{\partial f_i} = \frac{\partial \mathcal{L}_{i \rightarrow t}}{\partial s_t} \frac{\partial s_t}{\partial f_i}, \quad \frac{\partial \mathcal{L}_{i \rightarrow t}}{\partial s_t} = \frac{1}{\tau} (p_t - 1), \quad (5)$$

with p_t the softmax probability for the positive text t and $s_t = \text{sim}(f_i, g_t)$. The gradient of the similarity for the positive image-text pair (f_i, g_t) with respect to the pre-projection image feature f_i is given by:

$$\frac{\partial s_t}{\partial f_i} = \alpha_{t,i} \overbrace{W_i^\top W_t}^{\Psi} g_t - s_t \frac{\overbrace{W_i^\top W_i}^{\Psi_i} f_i}{\|W_i f_i\|_2^2}, \quad (6)$$

where $\alpha_{t,i}$ is a normalization factor. The full derivation is provided in the Supplementary Material (Sec. A).

This expression admits a clear interpretation: during training, the loss drives the image feature f_i toward its paired text feature g_t , first projected into the shared space by W_t and then pulled back into the image space by W_i^\top . The operator $\Psi = W_i^\top W_t$ therefore acts as an *inter-modal operator*, responsible for aligning image and text embeddings. The second term involves $\Psi_i = W_i^\top W_i$, an *intra-modal operator* which only enforces unit-norm constraints

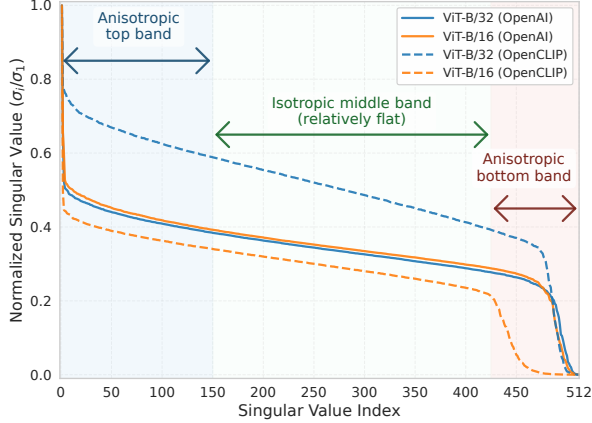


Figure 2. Spectra of the inter-modal operator $\Psi = W_i^\top W_t$ for CLIP ViT-B/16 and ViT-B/32 with OpenAI and DataComp (OpenCLIP) pre-training. Despite variations across models, all spectra show pronounced anisotropy in the extreme top and bottom singular directions, while staying relatively flat in the middle band.

on image features but does not induce attraction between image features. Thus, during CLIP training, images interact with text via the inter-modal operator Ψ , encouraging inter-modal alignment. The only intra-modal interactions (via Ψ_i) are between an image and *itself*, which do nothing to promote intra-modal alignment. Nevertheless, Ψ_i implicitly defines the cosine similarity used in image-to-image retrieval or classification between image features f_i and $f_{\hat{i}}$:

$$\text{sim}(f_i, f_{\hat{i}}) = \frac{f_i^\top (W_i^\top W_i) f_{\hat{i}}}{\|W_i f_i\|_2 \|W_i f_{\hat{i}}\|_2} = \frac{f_i^\top \Psi_i f_{\hat{i}}}{\|W_i f_i\|_2 \|W_i f_{\hat{i}}\|_2}, \quad (7)$$

even though it is not trained to align images, making it sub-optimal for modeling image-to-image relationships.

3.2. Spectral Analysis of the Inter-modal Operator

From the previous discussion, $\Psi = W_i^\top W_t$ and its transpose $\Psi^\top = W_t^\top W_i$ define a pair of linear mappings that connect the pre-projection spaces of the two modalities. To analyze the distortion introduced by these operators, we compute the Singular Value Decomposition (SVD) of Ψ :

$$\Psi = U \Sigma V^\top. \quad (8)$$

where $U \in \mathbb{R}^{d_i \times d}$ contains the left singular vectors spanning the output (image) space, and $V \in \mathbb{R}^{d_t \times d}$ contains the right singular vectors spanning the input (text) space. The diagonal matrix $\Sigma \in \mathbb{R}^{d \times d}$ contains the singular values, which quantify how directions in one modality are stretched or compressed when mapped to the other through Ψ or Ψ^\top . It suffices to analyze Ψ , as Ψ^\top shares the same singular values; the SVD of Ψ^\top simply exchanges the roles of the input and output spaces without altering the spectrum.

In Fig. 2 we see that the singular values are relatively flat across a broad central region, while exhibiting strong anisotropy in both the top and bottom parts of the spectrum. The extensive, relatively flat region in the middle reveals an approximately *isotropic* subspace in which features can be transferred across modalities with minimal distortion. This suggests the presence of a shared semantic subspace *directly identifiable from the projector weights themselves*. Conversely, the top and bottom directions capture modality-specific variations which we analyze in the next section.

Building on these observations, we now investigate whether this shared semantic subspace learned by CLIP can be exploited to improve intra-modal alignment when CLIP is used in intra-modal settings.

4. IsoCLIP: Aligning Projector Weights by Decomposing the Inter-modal Operator

The analysis in Sec. 3.1 suggests that intra-modal similarities in CLIP rely on a geometry induced by the intra-modal operator $\Psi_i = W_i^\top W_i$ which is not optimized during training (Eqs. (6), (7)). We therefore investigate whether the inter-modal operator Ψ , optimized during training, can reveal shared semantic directions across modalities for improved intra-modal similarity. We decompose the inter-modal operator as $\Psi = U \Sigma V^\top$, where U, V span the image and text spaces and Σ contains singular values in decreasing order. We then restrict Ψ to the relatively flat central region of its spectrum Σ by retaining only the corresponding singular directions. Formally, we select the paired subspaces:

$$\begin{aligned} \mathcal{S}_U &= \text{span}\{u_j | j \in [k_t, r - k_b]\} \text{ and} \\ \mathcal{S}_V &= \text{span}\{v_j | j \in [k_t, r - k_b]\}, \end{aligned} \quad (9)$$

where u_j and v_j identify the j -th column of U and V respectively, r is the rank of Ψ , and k_t and k_b delimit the range of approximately isotropic singular values. Projecting the image and text projectors onto these subspaces yields:

$$\widehat{W}_i = W_i U_{\mathcal{S}_U} U_{\mathcal{S}_U}^\top, \quad \widehat{W}_t = W_t V_{\mathcal{S}_V} V_{\mathcal{S}_V}^\top. \quad (10)$$

This projection defines our approach, IsoCLIP. This operation, via the orthogonal projectors $U_{\mathcal{S}_U} U_{\mathcal{S}_U}^\top$ and $V_{\mathcal{S}_V} V_{\mathcal{S}_V}^\top$, restricts W_i and W_t to the middle-band of the inter-modal operator Ψ , filtering out the anisotropic top and bottom directions and aligning both mappings to a shared semantic space. The resulting projectors \widehat{W}_i and \widehat{W}_t therefore operate in a common basis, corresponding to the subspace where image and text representations exhibit minimal distortion. For intra-modal tasks, the IsoCLIP projectors are used to compute the cosine similarities within the isotropic subspace. For image-to-image retrieval or classification, the similarities between images i and \hat{i} are computed as:

$$\text{sim}(f_i, f_{\hat{i}}) = \frac{f_i^\top (\widehat{W}_i^\top \widehat{W}_i) f_{\hat{i}}}{\|\widehat{W}_i f_i\|_2 \|\widehat{W}_i f_{\hat{i}}\|_2}, \quad (11)$$

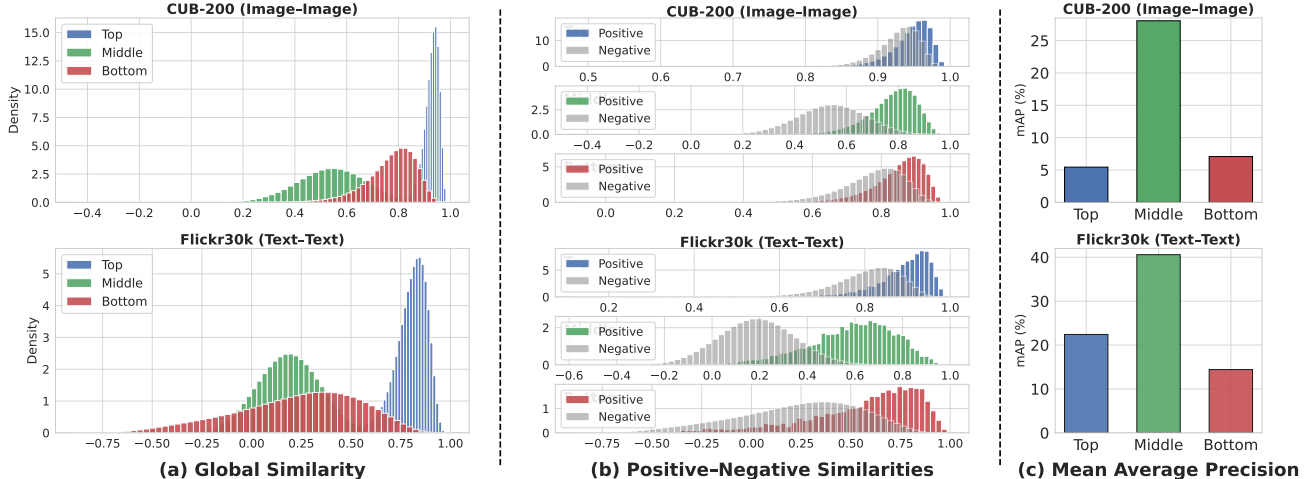


Figure 3. Investigation of different regions of the spectrum (top 50, middle 50, and bottom 50 directions) of the inter-modal operator Ψ for aligning the CLIP Projector weights, as defined in Eq. (10), utilizing the ViT-B/16 model for both image-to-image and text-to-text retrieval tasks. (a) Analysis of cosine similarity distributions showing very high similarities for the top band, and more well-behaved distributions for middle and bottom bands. (b) Overlap between cosine similarities of positive and negative pairs showing better separation for the middle band but highly overlapping distributions for top and bottom bands, implying higher intra-modal misalignment. (c) Performance comparison showing far superior performance using the well-aligned middle band compared to top and bottom bands.

and analogously for text-to-text retrieval using \widehat{W}_t . Using \widehat{W}_i for intra-modal similarity flattens the spectrum of $W_i^\top W_i$ (Eq. 7), spreading similarity across more directions, improving positive-negative separation, and raising mAP. See Sec. B of the Supplementary Material for details.

Semantics of the middle band of the spectrum. The singular directions associated with the middle band of the spectrum $[k_t, r - k_b]$ (see Eq. (9)) contain the shared semantic directions that support CLIP’s inter-modal alignment. To investigate this hypothesis, we isolate three spectral regions in ViT-B/16 – the *top interval* $[0, k_t]$, the *bottom interval* $[r - k_b, r]$, and a *middle band* defined symmetrically around midpoint of the spectrum, $[r/2 - k_t/2, r/2 + k_b/2]$, where r is the rank and $k_t = k_b = 50$. This choice is motivated by the singular value profile in Fig. 2, which shows sharp slope changes in the first and last ~ 50 components, while the central region is comparatively flat and thus expected to encode more semantic structure. Here we use 50 dimensions for the bands for analysis. See Sec. 5.3 for a discussion of how optimal values are selected in all experiments.

We restrict the projection matrix of the image and text encoder to each subspace (Eq. (10)) and analyze how the cosine similarities between query and gallery features change when only the top, middle, or bottom directions are used. Fig. 3 summarizes the effect on global and positive-negative similarity distributions, and retrieval performance for both image-to-image and text-to-text retrieval. We see that:

- **Top directions** inflate cosine similarities (Fig. 3a) but mix positive and negative pairs (Fig. 3b), which leads to poor retrieval performance (Fig. 3c).

- **Bottom directions** produce less inflated similarities (Fig. 3a) but still fail to separate positives from negatives (Fig. 3b), resulting in poor performance (Fig. 3c).
- **Middle directions**, in contrast, yield well-behaved similarity distributions (Fig. 3a, 3b) and consistently superior retrieval accuracy across modalities (Fig. 3c).

An interesting observation is the *asymmetric effect across modalities*: top directions are more detrimental to image retrieval than to text retrieval, while bottom directions show the opposite trend (Fig. 3c). This pattern suggests that the spectral extremes capture *modality-specific variation*, with the top directions predominantly text-specific and the bottom ones predominantly image-specific. Both extremes are detrimental for intra-modal tasks, whereas the middle band encodes the semantic subspace that both modalities rely on and is more discriminative for intra-modal tasks. See the Supplementary Material (Sec. C) for additional evidence.

Extension to non-linear projector heads. From Eq. 10 it is clear that IsoCLIP applies directly to CLIP-style models with linear projection heads. For models such as SigLIP2 [42], which employ a non-linear image-projection, IsoCLIP can be extended via a first-order linearization of the projection head [47]. In Sec. D of the Supplementary Materials we provide details of the proposed linearization.

5. Experimental Results

In this section we report on experiments evaluating IsoCLIP in a range of intra-modal settings, employing several VLMs, and on a diverse selection of benchmark datasets.

Table 1. **Image-to-image retrieval** performance for multiple CLIP models on 13 datasets. We also report the query latency for all methods.

Method	Intra-modal	Backbone	Latency (ms)	Caltech	CUB	ROxford	RParis	Cars	Pets	Flowers	Aircraft	DTD	EuroSAT	Food101	SUN397	UCF101	Avg
Image-Image	✓	ViT-B/32	7 ± 1	77.1	22.9	42.6	67.9	24.6	30.5	62.0	<u>14.5</u>	28.1	47.9	32.3	34.3	47.1	40.9
OTI (I→T)	✗		1879 ± 35	<u>79.9</u>	<u>24.6</u>	<u>43.0</u>	<u>70.3</u>	<u>28.0</u>	<u>37.5</u>	<u>62.6</u>	14.4	31.9	<u>47.2</u>	<u>34.7</u>	<u>36.3</u>	48.6	43.0
IsoCLIP	✓		7 ± 1	80.8	27.0	47.2	73.8	30.0	40.8	66.5	14.9	<u>30.9</u>	51.5	38.0	36.4	<u>48.4</u>	45.1
Image-Image	✓	ViT-B/16	6 ± 1	80.6	31.6	46.6	75.3	31.0	36.3	70.8	19.0	30.7	51.2	42.8	35.9	49.8	46.3
OTI (I→T)	✗		1856 ± 56	<u>83.5</u>	<u>33.9</u>	<u>49.9</u>	<u>77.4</u>	<u>37.2</u>	<u>42.9</u>	<u>72.8</u>	<u>20.1</u>	<u>35.1</u>	<u>50.5</u>	<u>47.5</u>	38.7	<u>52.6</u>	49.4
IsoCLIP	✓		6 ± 1	85.0	38.6	51.8	82.0	41.2	50.7	77.4	20.5	36.0	55.6	53.5	<u>38.5</u>	55.4	52.8
Image-Image	✓	ViT-L/14	11 ± 1	83.2	43.0	57.5	76.9	43.3	47.3	84.0	25.8	34.1	59.0	53.0	39.1	60.0	54.3
OTI (I→T)	✗		1872 ± 91	87.3	<u>47.1</u>	<u>62.4</u>	<u>77.1</u>	<u>50.5</u>	<u>56.0</u>	<u>86.0</u>	<u>27.1</u>	<u>37.7</u>	<u>56.3</u>	<u>55.9</u>	43.5	62.8	57.7
IsoCLIP	✓		11 ± 1	<u>87.0</u>	52.2	66.4	81.4	56.4	63.5	88.2	28.2	39.0	61.6	62.9	<u>41.0</u>	<u>61.9</u>	60.7
Image-Image	✓	ViT-B/16-open	6 ± 1	85.7	42.8	65.3	83.2	55.8	50.4	84.6	23.1	39.9	57.8	51.1	39.5	52.9	56.3
OTI (I→T)	✗		1836 ± 83	<u>85.8</u>	<u>45.1</u>	69.5	85.8	<u>60.5</u>	<u>56.5</u>	<u>85.2</u>	<u>23.4</u>	43.1	58.8	<u>54.4</u>	40.8	54.1	58.7
IsoCLIP	✓		6 ± 1	87.6	45.9	<u>67.3</u>	<u>85.0</u>	60.7	57.8	85.8	23.5	<u>42.5</u>	<u>58.6</u>	54.7	<u>39.3</u>	<u>53.4</u>	<u>58.6</u>
Image-Image	✓	PE-Core-B-16	8 ± 1	89.1	48.9	61.6	83.4	53.4	57.1	85.0	31.7	39.0	55.1	53.4	43.9	60.3	58.6
OTI (I→T)	✗		3252 ± 35	<u>90.5</u>	<u>51.5</u>	<u>65.7</u>	<u>85.2</u>	<u>60.2</u>	<u>62.9</u>	<u>87.2</u>	<u>32.7</u>	43.5	56.9	<u>55.8</u>	<u>44.9</u>	63.0	<u>61.5</u>
IsoCLIP	✓		8 ± 1	91.6	53.0	67.0	86.5	62.3	68.2	88.0	34.9	<u>43.1</u>	<u>56.3</u>	57.6	45.2	<u>62.1</u>	62.8

Table 2. **Text-to-text retrieval** performance for multiple CLIP models on three datasets.

Method	Intra-modal	Backbone	Latency (ms)	COCO	Flickr30k	nocaps	Avg
Text-Text	✓	ViT-B/32	6 ± 1	26.2	51.7	35.1	37.7
OVI (T→I)	✗		11549 ± 192	<u>28.3</u>	<u>54.8</u>	<u>38.8</u>	<u>40.6</u>
IsoCLIP	✓		6 ± 1	29.1	56.8	39.6	41.9
Text-Text	✓	ViT-B/16	6 ± 1	26.1	50.7	35.1	37.3
OVI (T→I)	✗		11929 ± 125	<u>28.2</u>	<u>53.1</u>	<u>38.3</u>	<u>39.9</u>
IsoCLIP	✓		6 ± 1	28.9	55.2	39.4	41.2
Text-Text	✓	ViT-L/14	6 ± 1	26.7	52.3	35.7	38.2
OVI (T→I)	✗		21366 ± 33	<u>29.4</u>	<u>54.9</u>	<u>39.5</u>	<u>41.3</u>
IsoCLIP	✓		6 ± 1	30.1	58.6	40.4	43.0
Text-Text	✓	ViT-B/16-open	6 ± 1	29.8	57.0	40.0	42.3
OVI (T→I)	✗		11822 ± 169	31.9	<u>60.2</u>	43.7	45.3
IsoCLIP	✓		6 ± 1	31.9	60.8	<u>43.3</u>	45.3

5.1. Experimental Settings

We evaluate our method on a wide range of datasets and models covering both *image-to-image* and *text-to-text* retrieval, following the protocol of Mistretta et al. [25].

Datasets and metrics. We evaluate image-to-image retrieval and image classification on a wide range of datasets, including fine-grained, scene-level, and object-centric benchmarks. For text-to-text retrieval, we use three caption datasets following Mistretta et al. [25]. See Sec. E of the Supplementary Material for full dataset details. For retrieval experiments, we report the *mean average precision* (mAP), while for the image classification performance, we report the *accuracy*. We also report the time taken to encode a single query using the three methods (averaged over 20 runs) as the latency in milliseconds.

Backbones. We conduct experiments using multiple CLIP variants with different backbones and pre-training datasets. Specifically, we consider *OpenAI CLIP* models with ViT-B/32, ViT-B/16, and ViT-L/14 image backbones, as well as *OpenCLIP* models (ViT-B/16-open) trained on the DataComp dataset. To further explore vision-language models

distinct from CLIP, we use the recent *Perception-Encoder* (PE) model [3] pre-trained on the PE Video Dataset [3], allowing us to analyze generalization across diverse vision–language representations. In the Supplementary Material (Sec. F) we extend the evaluation to additional models, including ViT-B/32-open, EVA-02 [8], and SigLIP2 B/16.

Middle band selection. Since architectures vary in both the number of singular directions and shape of their spectra (Fig. 2), the optimal k_t and k_b differ across models. We empirically select the top k_t and bottom k_b spectral components to remove, as defined in Eq. (9), based on a single dataset for all backbones. For image-based tasks we validate these hyperparameters on image-to-image retrieval using Caltech101, a generic object recognition dataset. These parameters are used for all other datasets in image retrieval and classification experiments. For text-to-text retrieval, we validate these hyperparameters on COCO and use them for all other text datasets. In Sec. 5.3 we discuss the impact of hyperparameter selection.

5.2. Comparison with Standard and Inversion-based Approaches

In this section we evaluate IsoCLIP on image-to-image retrieval and text-to-text retrieval.

Image-to-image retrieval. We compare IsoCLIP against standard image-to-image retrieval (Image-Image) using the vision encoder only, and against the existing textual inversion-based approach (OTI). OTI maps the query image features into the text space by performing 150 steps of optimization and then retrieves from the image gallery, following [25]. By inverting an image into a text embedding, OTI compares the inverted pseudo-text query against the gallery image embeddings, resulting in an inter-modal comparison and thereby circumventing intra-modal misalignment.

In Tab. 1 we see that IsoCLIP significantly improves the performance over standard image-to-image retrieval by sig-

Table 3. **Image classification** performance for multiple CLIP models on 10 datasets. We compare IsoCLIP with intra-modal NCM classification. Zero-shot results are reported only for reference, as they do not require training images to compute class prototypes.

Method	Intra-modal	Classifier	Backbone	Caltech	Cars	Pets	Flowers	Aircraft	DTD	EuroSAT	Food101	SUN397	UCF101	Average
Image-Text	✗	Zero-Shot		91.2	60.4	87.5	67.0	19.1	43.6	45.2	80.5	62.0	62.0	61.9
Image-Image	✓	NCM	ViT-B/32	91.9	67.0	77.1	93.7	34.5	64.4	77.7	77.3	70.2	76.6	73.0
IsoCLIP	✓	NCM		93.0	73.0	84.0	93.8	35.0	66.8	80.6	78.6	70.5	77.8	75.3
Image-Text	✗	Zero-Shot		92.9	65.3	89.1	71.4	24.8	44.4	47.8	86.1	62.6	66.7	65.1
Image-Image	✓	NCM	ViT-B/16	94.1	74.8	84.2	96.2	43.6	65.8	79.2	84.0	72.1	80.2	77.4
IsoCLIP	✓	NCM		95.4	81.2	90.9	97.1	45.6	68.4	82.6	85.6	72.0	81.7	80.1
Image-Text	✗	Zero-Shot		94.8	76.8	93.6	79.3	32.5	53.1	58.1	91.0	67.6	74.2	72.1
Image-Image	✓	NCM	ViT-L/14	96.8	83.7	91.8	98.8	55.5	70.4	84.7	90.0	76.7	85.9	83.4
IsoCLIP	✓	NCM		97.2	87.8	94.4	99.0	58.0	72.9	88.5	90.8	75.8	86.9	85.1

nificant margins across all backbones (6.5% on ViT-B/16, and 4.2% on Perception-Encoder on average). IsoCLIP outperforms OTI with significantly less query latency on all backbones except ViT-B/16-open where it performs similar to OTI. The improved performance of IsoCLIP compared to standard CLIP Image-Image confirms the potential of using the modality-aligned directions for intra-modal tasks.

Text-to-text retrieval. We compare IsoCLIP with standard text-to-text retrieval using the text encoder only (Text-Text), and against the existing visual inversion-based approach (OVI). OVI maps the query text feature into the image space by performing 1000 optimization steps and then retrieves from the text gallery [25]. Converting a text query into an image embedding, OVI results in an inter-modal comparison and circumvents intra-modal misalignment.

We report in Tab. 2 the comparison of IsoCLIP with standard text-to-text retrieval and OVI. We observe that IsoCLIP outperforms standard retrieval significantly on all datasets (3.9% using ViT-B/16, 4.8% using ViT-L/14 on average). Despite having negligible latency compared to OVI, IsoCLIP performs similar or better than OVI in most settings.

5.3. Analysis and Ablations

Analysis on Image classification. Existing works [16, 43, 55, 56] use intra-modal comparisons alongside textual information for CLIP-based image classification. To evaluate IsoCLIP in an intra-modal classification setting, we adopt the Nearest Class Mean (NCM) classifier [13], which classifies images by their proximity to class prototypes computed from all training data.

Specifically, we compute the mean of the pre-projection image features for each class and then project them to the shared embedding space using the IsoCLIP image projector. These projected class means are used as prototypes for classification instead of the text embeddings used for zero-shot classification. At inference time, the test image embeddings generated using the IsoCLIP image projector will be assigned to the class whose prototype has the highest cosine similarity to the test image.

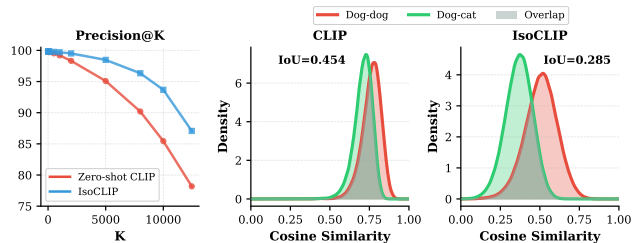


Figure 4. Analysis on *Dogs vs. Cats* [7]. (left) IsoCLIP achieves higher precision than CLIP as the number of retrieved dog images K increases. (center) CLIP shows significant overlap between intra-class (dog-dog) and inter-class (dog-cat) similarities due to intra-modal misalignment. (right) IsoCLIP reduces this overlap, making image-image similarities more discriminative.

We report in Tab. 3 the performance of IsoCLIP and compare to standard image-to-image classification using NCM classifiers. The NCM classifier significantly outperforms the inter-modal zero-shot classifier (having access only to text class names) on most datasets, as it leverages the entire training set of images to compute the prototypes. On an average, IsoCLIP outperforms standard image-to-image classification significantly across three different backbones. This implies that IsoCLIP could also be exploited for classification tasks involving intra-modal comparisons.

Analysis of intra-modal misalignment. To study how much IsoCLIP improves intra-modal alignment in a controlled and isolated setting, we evaluate on the *Dogs vs. Cats* dataset which contains 25K images [7]. Following the preprocessing from [25], we remove dog images that are closer to “A photo of a cat” than to “A photo of a dog”. This gives us a perfect inter-modally aligned subset of images, which ensures that an improvement in image-to-image retrieval performance arises only from mitigation of intra-modal misalignment.

We perform image-to-image retrieval with ViT-B/16 using dog images as queries and cats and dogs as gallery. In Fig. 4 we show that IsoCLIP outperforms CLIP when varying the number of retrieved samples K in terms

Table 4. **Ablation Study.** We compare IsoCLIP against using pre-projection image features for retrieval (Image-Image [Pre]) and against whitening the CLIP image projection weights (W_i^{white}).

Method	Backbone	Caltech	CUB	ROxford	RParis	Cars	Pets	Flowers	Aircraft	DTD	EuroSAT	Food101	SUN397	UCF101	Average
Image-Image		80.6	31.6	46.6	75.3	31.0	36.3	70.8	19.0	30.7	51.2	42.8	35.9	49.8	46.3
Image-Image [Pre]	ViT-B/16	81.6	32.7	49.2	77.8	32.0	39.0	72.4	19.4	32.5	54.5	45.3	38.8	54.2	48.4
W_i^{white}		82.1	34.4	48.5	78.6	34.2	40.8	73.7	19.5	32.9	54.3	46.5	38.2	53.9	49.0
IsoCLIP		85.0	38.6	51.8	82.0	41.2	50.7	77.4	20.5	36.0	55.6	53.5	38.5	55.4	52.8
Image-Image		83.2	43.0	57.5	76.9	43.3	47.3	84.0	25.8	34.1	59.0	53.0	39.1	60.0	54.3
Image-Image [Pre]	ViT-L/14	85.4	42.6	59.5	78.1	41.9	48.0	84.7	25.9	35.3	61.7	54.6	42.0	61.9	55.5
W_i^{white}		85.6	44.0	60.1	77.6	44.2	49.2	85.3	26.1	35.7	61.3	55.1	41.6	61.9	56.0
IsoCLIP		87.0	52.2	66.4	81.4	56.4	63.5	88.2	28.2	39.0	61.6	62.9	41.0	61.9	60.7

of Precision@K. We demonstrate that the similarities between positives (Dog-to-Dog) and between negatives (Dog-to-Cat) overlap more in the CLIP embedding space (IoU=0.464) compared to IsoCLIP (IoU=0.293) – a clear visualization of intra-modal alignment induced by IsoCLIP.

Ablation studies. We evaluate two additional strategies to better understand the contribution of the image projection head to intra-modal misalignment (see Sec. 3.1). Since intra-modal misalignment clearly manifests when using post-projection features $W_i f_i$ (Image-Image), we also evaluate retrieval performance using the *raw pre-projection features* f_i (Image-Image [Pre]). This ablation tests whether the projection head itself is responsible for the suboptimal performance in intra-modal similarity comparisons. We also evaluate a whitened image projector obtained by decomposing $W_i = U_i \Sigma_i V_i^T$ and constructing $W_i^{\text{white}} = U_i V_i^T$. This flattens the spectrum of W_i , while preserving its directions, allowing us to test whether a uniform spectrum is sufficient to mitigate intra-modal misalignment.

Tab. 4 shows that both ablations yield significant improvement over the standard Image-Image baseline: +2.1 mAP (Image-Image [Pre]) and +2.7 mAP (W_i^{white}) on ViT-B/16, and +1.2 and +2.7 respectively on ViT-L/14. These improvements indicate that the projector introduces significant anisotropy that harms intra-modal retrieval.

IsoCLIP achieves larger gains than both alternatives. Since the isotropic middle band of Ψ captures the semantic directions underlying image-text alignment, restricting the projector to this subspace is more effective than either flattening the spectrum (whitening) or bypassing the projection head (Image-Image [Pre]). See Supplementary Material (Sec. F) for results on other models.

Selection of k_t and k_b . We select k_t and k_b , which define the middle isotropic band in IsoCLIP, for each backbone using Caltech101 (image-to-image retrieval) and COCO (text-to-text retrieval), and apply these values to all other datasets. See Sec. G of the Supplementary Material for details.

In Fig. 5 we analyze the selection for ViT-B/16. On Caltech101, for $k_b = 50$ the mAP improves more when varying k_t from 0 to 200 (about 5%), while for $k_t = 200$, mAP improves by about 2% when varying k_b . This implies that

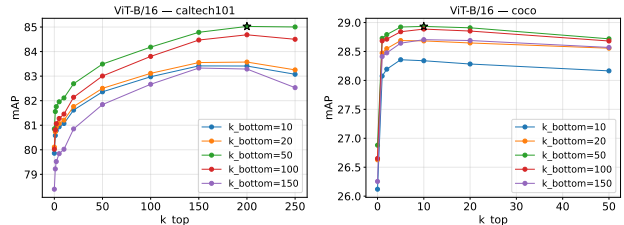


Figure 5. Ablation showing the impact of varying the k_t and k_b values for the isotropic middle band selection on Caltech101 (image-to-image retrieval) and COCO (text-to-text retrieval).

removing the top directions is more impactful for image-based tasks as shown in Fig. 3. On COCO, we observe that the removal of only a few directions ($k_t = 10, k_b = 50$) is sufficient to improve the performance for text-based tasks.

6. Conclusions

In this paper we explored several aspects of CLIP, focusing on the role of the projectors in intra-modal misalignment. We rendered explicit an inter-modal operator hidden in CLIP responsible for aligning image and text representations, and identified a second, intra-modal operator that enforces normalization but does not promote intra-modal alignment. Based on this, we identify a well-aligned subspace characterized by the spectrum of the inter-modal operator Ψ , and proposed mapping projector weights onto this shared subspace to suppress anisotropic directions before embedding into the shared CLIP space. Our experiments demonstrate that, on the intra-modal tasks of image retrieval and text retrieval, IsoCLIP outperforms existing methods, induces better intra-modal alignment, and adds no latency.

Limitations and Future Works. Using the IsoCLIP projectors degrades performance on inter-modal tasks such as text-to-image retrieval (see Sec. H of the Supplementary Material for a discussion). Moreover, we empirically select hyperparameters k_t and k_b based on a single dataset for each modality, and we believe that more principled approaches for band selection should be explored in future work.

Acknowledgments

This work was supported by Grants PID2022-143257NB-I00, and AIA2025-163919-C52 funded by MCIN/AEI/10.13039/501100011033 and the FEDER, and by the European Union Horizon Europe research and innovation programme under grant agreement number 101214398 (ELLIOT) and the AI4DeBunk project (HORIZON-CL4-2023-HUMAN-01-CNECT grant n.101135757). Bartłomiej Twardowski acknowledges the grant RYC2021-032765-I and National Centre of Science (NCN, Poland) Grant No. 2023/51/D/ST6/02846.

References

- [1] Harsh Agrawal, Karan Desai, Yufei Wang, Xinlei Chen, Rishabh Jain, Mark Johnson, Dhruv Batra, Devi Parikh, Stefan Lee, and Peter Anderson. nocaps: novel object captioning at scale. In *Proceedings of the IEEE International Conference on Computer Vision*, pages 8948–8957, 2019. 17
- [2] Alberto Baldrati, Marco Bertini, Tiberio Uricchio, and Alberto Del Bimbo. Effective conditioned and composed image retrieval combining clip-based features. In *Proceedings of the IEEE/CVF conference on computer vision and pattern recognition*, pages 21466–21474, 2022. 1
- [3] Daniel Bolya, Po-Yao Huang, Peize Sun, Jang Hyun Cho, Andrea Madotto, Chen Wei, Tengyu Ma, Jiale Zhi, Jathushan Rajasegaran, Hanoona Abdul Rasheed, Junke Wang, Marco Monteiro, Hu Xu, Shiyu Dong, Nikhila Ravi, Shang-Wen Li, Piotr Dollar, and Christoph Feichtenhofer. Perception encoder: The best visual embeddings are not at the output of the network. In *The Thirty-ninth Annual Conference on Neural Information Processing Systems*, 2025. 2, 6
- [4] Lukas Bossard, Matthieu Guillaumin, and Luc Van Gool. Food-101—mining discriminative components with random forests. In *Computer Vision—ECCV 2014: 13th European Conference, Zurich, Switzerland, September 6–12, 2014, Proceedings, Part VI 13*, pages 446–461. Springer, 2014. 17
- [5] Lorenzo Caselli, Marco Mistretta, Simone Magistri, and Andrew D. Bagdanov. SpectralGCD: Spectral concept selection and cross-modal representation learning for generalized category discovery. In *The Fourteenth International Conference on Learning Representations*, 2026. 1
- [6] Mircea Cimpoi, Subhansu Maji, Iasonas Kokkinos, Sammy Mohamed, and Andrea Vedaldi. Describing textures in the wild. In *Proceedings of the IEEE conference on computer vision and pattern recognition*, pages 3606–3613, 2014. 17
- [7] Jeremy Elson, John R Douceur, Jon Howell, and Jared Saul. Asirra: a captcha that exploits interest-aligned manual image categorization. *CCS*, 7:366–374, 2007. 7
- [8] Yuxin Fang, Quan Sun, Xinggang Wang, Tiejun Huang, Xinlong Wang, and Yue Cao. Eva-02: A visual representation for neon genesis. *Image and Vision Computing*, 149:105171, 2024. 6, 18
- [9] Li Fei-Fei, Rob Fergus, and Pietro Perona. Learning generative visual models from few training examples: An incremental bayesian approach tested on 101 object categories. In *2004 conference on computer vision and pattern recognition workshop*, pages 178–178. IEEE, 2004. 17
- [10] Rinon Gal, Yuval Alaluf, Yuval Atzmon, Or Patashnik, Amit Haim Bermano, Gal Chechik, and Daniel Cohen-Or. An image is worth one word: Personalizing text-to-image generation using textual inversion. In *The Eleventh International Conference on Learning Representations*, 2023. 1
- [11] Yossi Gandelsman, Alexei A Efros, and Jacob Steinhardt. Interpreting CLIP’s image representation via text-based decomposition. In *The Twelfth International Conference on Learning Representations*, 2024. 2
- [12] Robert Geirhos, Priyank Jaini, Austin Stone, Sourabh Medapati, Xi Yi, George Toderici, Abhijit Ogale, and Jonathon Shlens. Towards flexible perception with visual memory. In *Proceedings of the 42nd International Conference on Machine Learning*, pages 19056–19081. PMLR, 2025. 1
- [13] Samantha Guerriero, Barbara Caputo, and Thomas Mensink. Deepncm: Deep nearest class mean classifiers. In *International Conference on Learning Representations - Workshop (ICLRw)*, 2018. 7
- [14] Zhongrui Gui, Shuyang Sun, Runjia Li, Jianhao Yuan, Zhaochong An, Karsten Roth, Ameya Prabhu, and Philip Torr. kNN-CLIP: Retrieval enables training-free segmentation on continually expanding large vocabularies. *Transactions on Machine Learning Research*, 2024. 1, 2
- [15] Patrick Helber, Benjamin Bischke, Andreas Dengel, and Damian Borth. Eurosat: A novel dataset and deep learning benchmark for land use and land cover classification. *IEEE Journal of Selected Topics in Applied Earth Observations and Remote Sensing*, 12(7):2217–2226, 2019. 17
- [16] Yunshi Huang, Fereshteh Shakeri, Jose Dolz, Malik Boudiaf, Houda Bahig, and Ismail Ben Ayed. Lp++: A surprisingly strong linear probe for few-shot clip. In *Proceedings of the IEEE/CVF Conference on Computer Vision and Pattern Recognition*, pages 23773–23782, 2024. 7
- [17] Andrej Karpathy and Li Fei-Fei. Deep visual-semantic alignments for generating image descriptions. In *Proceedings of the IEEE conference on computer vision and pattern recognition*, pages 3128–3137, 2015. 17
- [18] Giorgos Kordopatis-Zilos, Vladan Stojnić, Anna Manko, Pavel Suma, Nikolaos-Antonios Ypsilantis, Nikos Efthymiadis, Zakaria Laskar, Jiri Matas, Ondrej Chum, and Giorgos Tolias. Ilias: Instance-level image retrieval at scale. In *Proceedings of the Computer Vision and Pattern Recognition Conference*, pages 14777–14787, 2025. 1, 3
- [19] Jonathan Krause, Michael Stark, Jia Deng, and Li Fei-Fei. 3d object representations for fine-grained categorization. In *Proceedings of the IEEE international conference on computer vision workshops*, pages 554–561, 2013. 17
- [20] Meir Yossef Levi and Guy Gilboa. The double-ellipsoid geometry of CLIP. In *Forty-second International Conference on Machine Learning*, 2025. 2
- [21] Victor Weixin Liang, Yuhui Zhang, Yongchan Kwon, Serena Yeung, and James Y Zou. Mind the Gap: Understanding the Modality Gap in Multi-Modal Contrastive Representation Learning. *Advances in Neural Information Processing Systems*, 35:17612–17625, 2022. 2

- [22] Tsung-Yi Lin, Michael Maire, Serge Belongie, James Hays, Pietro Perona, Deva Ramanan, Piotr Dollár, and C Lawrence Zitnick. Microsoft coco: Common objects in context. In *Computer Vision—ECCV 2014: 13th European Conference, Zurich, Switzerland, September 6–12, 2014, Proceedings, Part V 13*, pages 740–755. Springer, 2014. 17
- [23] Yuyang Liu, Qiuhe Hong, Linlan Huang, Alexandra Gomez-Villa, Dipam Goswami, Xialei Liu, Joost van de Weijer, and Yonghong Tian. Continual learning for vlms: A survey and taxonomy beyond forgetting. *arXiv preprint arXiv:2508.04227*, 2025. 2
- [24] Subhransu Maji, Esa Rahtu, Juho Kannala, Matthew Blaschko, and Andrea Vedaldi. Fine-grained visual classification of aircraft. *arXiv preprint arXiv:1306.5151*, 2013. 17
- [25] Marco Mistretta, Alberto Baldrati, Lorenzo Agnolucci, Marco Bertini, and Andrew D. Bagdanov. Cross the gap: Exposing the intra-modal misalignment in CLIP via modality inversion. In *The Thirteenth International Conference on Learning Representations*, 2025. 1, 2, 3, 6, 7, 17
- [26] Norman Mu, Alexander Kirillov, David Wagner, and Saining Xie. Slip: Self-supervision meets language-image pre-training. In *European conference on computer vision*, pages 529–544. Springer, 2022. 2
- [27] Kengo Nakata, Youyang Ng, Daisuke Miyashita, Asuka Maki, Yu-Chieh Lin, and Jun Deguchi. Revisiting a knn-based image classification system with high-capacity storage. In *European conference on computer vision*, pages 457–474. Springer, 2022. 1, 3
- [28] Ryoya Nara, Yu-Chieh Lin, Yuji Nozawa, Youyang Ng, Goh Itoh, Osamu Torii, and Yusuke Matsui. Revisiting relevance feedback for clip-based interactive image retrieval. In *European Conference on Computer Vision*, pages 1–16. Springer, 2024. 1, 3
- [29] Maria-Elena Nilsback and Andrew Zisserman. Automated flower classification over a large number of classes. In *2008 Sixth Indian conference on computer vision, graphics & image processing*, pages 722–729. IEEE, 2008. 17
- [30] Maria Parrelli, Alexandros Delitzas, Nikolas Hars, Georgios Vlassis, Sotirios Anagnostidis, Gregor Bachmann, and Thomas Hofmann. Clip-guided vision-language pre-training for question answering in 3d scenes. In *Proceedings of the IEEE/CVF Conference on Computer Vision and Pattern Recognition*, pages 5607–5612, 2023. 1, 2
- [31] Omkar M Parkhi, Andrea Vedaldi, Andrew Zisserman, and CV Jawahar. Cats and dogs. In *2012 IEEE conference on computer vision and pattern recognition*, pages 3498–3505. IEEE, 2012. 17
- [32] Bryan A Plummer, Liwei Wang, Chris M Cervantes, Juan C Caicedo, Julia Hockenmaier, and Svetlana Lazebnik. Flickr30k entities: Collecting region-to-phrase correspondences for richer image-to-sentence models. In *Proceedings of the IEEE international conference on computer vision*, pages 2641–2649, 2015. 17
- [33] Filip Radenović, Ahmet Iscen, Giorgos Tolias, Yannis Avrithis, and Ondřej Chum. Revisiting oxford and paris: Large-scale image retrieval benchmarking. In *Proceedings of the IEEE conference on computer vision and pattern recognition*, pages 5706–5715, 2018. 17
- [34] Alec Radford, Jong Wook Kim, Chris Hallacy, Aditya Ramesh, Gabriel Goh, Sandhini Agarwal, Girish Sastry, Amanda Askell, Pamela Mishkin, Jack Clark, et al. Learning Transferable Visual Models From Natural Language Supervision. In *International conference on machine learning*, pages 8748–8763. PMLR, 2021. 1, 2
- [35] Nataniel Ruiz, Yuanzhen Li, Varun Jampani, Yael Pritch, Michael Rubinstein, and Kfir Aberman. Dreambooth: Fine tuning text-to-image diffusion models for subject-driven generation. In *Proceedings of the IEEE/CVF conference on computer vision and pattern recognition*, pages 22500–22510, 2023. 1
- [36] Aneeshan Sain, Ayan Kumar Bhunia, Pinaki Nath Chowdhury, Subhadeep Koley, Tao Xiang, and Yi-Zhe Song. Clip for all things zero-shot sketch-based image retrieval, fine-grained or not. In *Proceedings of the IEEE/CVF conference on computer vision and pattern recognition*, pages 2765–2775, 2023. 1, 2
- [37] Konstantin Schall, Kai Uwe Barthel, Nico Hezel, and Klaus Jung. Optimizing clip models for image retrieval with maintained joint-embedding alignment. In *International Conference on Similarity Search and Applications*, pages 97–110. Springer, 2024. 1, 3
- [38] Simon Schrodi, David T. Hoffmann, Max Argus, Volker Fischer, and Thomas Brox. Two effects, one trigger: On the modality gap, object bias, and information imbalance in contrastive vision-language models. In *The Thirteenth International Conference on Learning Representations*, 2025. 2
- [39] Peiyang Shi, Michael C Welle, Márten Björkman, and Danica Kragic. Towards Understanding the Modality Gap in CLIP. In *ICLR 2023 Workshop on Multimodal Representation Learning: Perks and Pitfalls*, 2023. 2
- [40] Haoyu Song, Li Dong, Weinan Zhang, Ting Liu, and Furu Wei. CLIP models are few-shot learners: Empirical studies on VQA and visual entailment. In *Proceedings of the 60th Annual Meeting of the Association for Computational Linguistics (Volume 1: Long Papers)*, pages 6088–6100, Dublin, Ireland, 2022. Association for Computational Linguistics. 1
- [41] Khurram Soomro, Amir Roshan Zamir, and Mubarak Shah. Ucf101: A dataset of 101 human actions classes from videos in the wild. *arXiv preprint arXiv:1212.0402*, 2012. 17
- [42] Michael Tschannen, Alexey Gritsenko, Xiao Wang, Muhammad Ferjad Naeem, Ibrahim Alabdulmohsin, Nikhil Parthasarathy, Talfan Evans, Lucas Beyer, Ye Xia, Basil Mustafa, Olivier Hénaff, Jeremiah Harmsen, Andreas Steiner, and Xiaohua Zhai. Siglip 2: Multilingual vision-language encoders with improved semantic understanding, localization, and dense features, 2025. 5, 16, 18
- [43] Vishaal Udandarao, Ankush Gupta, and Samuel Albanie. SuS-X: Training-Free Name-Only Transfer of Vision-Language Models. In *Proceedings of the IEEE/CVF International Conference on Computer Vision*, pages 2725–2736, 2023. 1, 3, 7
- [44] Grant Van Horn, Oisín Mac Aodha, Yang Song, Yin Cui, Chen Sun, Alex Shepard, Hartwig Adam, Pietro Perona, and

- Serge Belongie. The inaturalist species classification and detection dataset. In *Proceedings of the IEEE conference on computer vision and pattern recognition*, pages 8769–8778, 2018. 18
- [45] Catherine Wah, Steve Branson, Peter Welinder, Pietro Perona, and Serge Belongie. The caltech-ucsd birds-200-2011 dataset. 2011. 17
- [46] Enguang Wang, Zhimao Peng, Zhengyuan Xie, Fei Yang, Xialei Liu, and Ming-Ming Cheng. Get: Unlocking the multi-modal potential of clip for generalized category discovery. In *Proceedings of the Computer Vision and Pattern Recognition Conference (CVPR)*, pages 20296–20306, 2025. 1
- [47] Haoqi Wang, Tong Zhang, and Mathieu Salzmann. SINDER: Repairing the singular defects of dinov2. In *Proceedings of the European Conference on Computer Vision (ECCV)*, 2024. 5, 16
- [48] Tongzhou Wang and Phillip Isola. Understanding contrastive representation learning through alignment and uniformity on the hypersphere. In *International conference on machine learning*, pages 9929–9939. PMLR, 2020. 2
- [49] Longhui Wei, Lingxi Xie, Wengang Zhou, Houqiang Li, and Qi Tian. Mvp: Multimodality-guided visual pre-training. In *European conference on computer vision*, pages 337–353. Springer, 2022. 1
- [50] Han Xiao, Georgios Mastrapas, and Bo Wang. Jina clip: Your clip model is also your text retriever. In *Multimodal Foundation Model meets Embodied AI Workshop@ICML2024*, 2024. 1
- [51] Jianxiong Xiao, James Hays, Krista A Ehinger, Aude Oliva, and Antonio Torralba. Sun database: Large-scale scene recognition from abbey to zoo. In *2010 IEEE computer society conference on computer vision and pattern recognition*, pages 3485–3492. IEEE, 2010. 17
- [52] Chao Yi, Lu Ren, De-Chuan Zhan, and Han-Jia Ye. Leveraging Cross-Modal Neighbor Representation for Improved CLIP Classification. In *Proceedings of the IEEE/CVF Conference on Computer Vision and Pattern Recognition*, pages 27402–27411, 2024. 1, 3
- [53] Qihang Yu, Ju He, Xueqing Deng, Xiaohui Shen, and Liang-Chieh Chen. Convolutions die hard: Open-vocabulary segmentation with single frozen convolutional clip. *Advances in Neural Information Processing Systems*, 36:32215–32234, 2023. 1, 2
- [54] Xiaohua Zhai, Basil Mustafa, Alexander Kolesnikov, and Lucas Beyer. Sigmoid loss for language image pre-training. In *Proceedings of the IEEE/CVF International Conference on Computer Vision*, pages 11975–11986, 2023. 2
- [55] Ce Zhang, Simon Stepputtis, Katia Sycara, and Yaqi Xie. Dual prototype evolving for test-time generalization of vision-language models. *Advances in Neural Information Processing Systems*, 37:32111–32136, 2024. 7
- [56] Renrui Zhang, Wei Zhang, Rongyao Fang, Peng Gao, Kunchang Li, Jifeng Dai, Yu Qiao, and Hongsheng Li. Tip-adapter: Training-free adaption of clip for few-shot classification. In *European conference on computer vision*, pages 493–510. Springer, 2022. 1, 7
- [57] Bolei Zhou, Agata Lapedriza, Antonio Torralba, and Aude Oliva. Places: An image database for deep scene understanding. *Journal of Vision*, 17(10):296–296, 2017. 18
- [58] Kaiyang Zhou, Jingkang Yang, Chen Change Loy, and Ziwei Liu. Conditional prompt learning for vision-language models. In *Proceedings of the IEEE/CVF conference on computer vision and pattern recognition*, pages 16816–16825, 2022. 2

Supplementary Material

This supplementary material provides additional details and analyses that complement the main paper. We include the full gradient derivation of the CLIP loss (Sec. A), a detailed analysis of how IsoCLIP improves intra-modal retrieval (Sec. B), and an investigation of the effect of adding top and bottom spectral directions to the middle band (Sec. C). We then describe the extension of IsoCLIP to non-linear projection heads (Sec. D), followed by dataset descriptions and implementation details (Sec. E). Additional experimental results, ablations, and comparisons are reported in Sec. F. Finally, we discuss hyperparameter selection (Sec. G), inter-modal degradation (Sec. H), and provide the complete IsoCLIP algorithm pseudocode (Sec. I).

Table of Contents

A. Inter-Modal and Intra-Modal Operators: Gradient Derivation for the CLIP Loss

B. Improving Intra-Modal Retrieval via IsoCLIP

C. Adding Top and Bottom Directions to the Isotropic Middle Band Directions

D. Extension of IsoCLIP to non-linear projection heads

E. Dataset and Implementation Details

E.1. Datasets	
E.2. Implementation Details for Modality Inversion Baselines	

F. Additional Results and Ablations

F.1. Image-to-Image Retrieval on ViT-B/32-open, EVA-02 B/16 and SigLIP2 B/16	
F.2. Image Classification on ViT-B/16-open	
F.3. Comparison with Unimodal DINOv2 B/14	
F.4. Experiments on Places365 and iNaturalist	
F.5. Additional Ablations	

G. Analysis of Hyperparameter Selection

H. Inter-modal Degradation after Applying IsoCLIP

I. The IsoCLIP Algorithm

A. Inter-Modal and Intra-Modal Operators: Gradient Derivation for the CLIP Loss

The symmetric contrastive loss of CLIP is defined as:

$$\mathcal{L}_{\text{CLIP}} = \frac{1}{2}(\mathcal{L}_{i \rightarrow t} + \mathcal{L}_{t \rightarrow i}), \quad (\text{S1})$$

where $\mathcal{L}_{i \rightarrow t}$ moves the embedding of each image i toward the corresponding *positive* paired text t , while pushing it away from all other texts in the mini-batch. In the main paper we present the gradient contribution of the *positive* text g_t ; here we provide the complete derivation.

The loss $\mathcal{L}_{i \rightarrow t}$ is defined as:

$$\mathcal{L}_{i \rightarrow t} = -\log \frac{\exp(\text{sim}(f_i, g_t)/\tau)}{\sum_{t'} \exp(\text{sim}(f_i, g_{t'})/\tau)} = -\log \frac{\exp\left(\frac{f_i^\top (W_i^\top W_t) g_t / \tau}{\|W_i f_i\|_2 \|W_t g_t\|_2}\right)}{\sum_{t'} \exp\left(\frac{f_i^\top (W_i^\top W_t) g_{t'} / \tau}{\|W_i f_i\|_2 \|W_t g_{t'}\|_2}\right)}, \quad (\text{S2})$$

where f_i and g_t denote the pre-projection image and positive text feature respectively; W_i and W_t denote the image and text projector weights respectively; τ is the temperature; t denotes the *positive text* for image i , and t' ranges over the positive and negative texts in the mini-batch.

Defining the normalization factor

$$\alpha_{t,i} = \frac{1}{\|W_i f_i\|_2 \|W_t g_t\|_2}, \quad (\text{S3})$$

and the logit of the positive image–text pair

$$s_t = \alpha_{t,i} f_i^\top (W_i^\top W_t) g_t. \quad (\text{S4})$$

the loss becomes:

$$\mathcal{L}_{i \rightarrow t} = -\log \frac{\exp(s_t/\tau)}{\sum_{t'} \exp(s_{t'}/\tau)}.$$

By applying the chain rule and isolating the contribution of the *positive* text embedding, we obtain:

$$\frac{\partial \mathcal{L}_{i \rightarrow t}}{\partial f_i} = \frac{\partial \mathcal{L}_{i \rightarrow t}}{\partial s_t} \frac{\partial s_t}{\partial f_i}. \quad (\text{S5})$$

The first term is the standard derivative of cross-entropy with respect to the logit s_t :

$$\frac{\partial \mathcal{L}_{i \rightarrow t}}{\partial s_t} = \frac{1}{\tau} (p_t - 1), \quad \text{where} \quad p_t = \frac{\exp(s_t/\tau)}{\sum_{t'} \exp(s_{t'}/\tau)}$$

is the softmax probability of the positive text t .

For the second term, recalling the definitions in Eq. (S3) and Eq. (S4), we obtain

$$\frac{\partial s_t}{\partial f_i} = \alpha_{t,i} (W_i^\top W_t) g_t + \frac{\partial \alpha_{t,i}}{\partial f_i} f_i^\top (W_i^\top W_t) g_t = \alpha_{t,i} (W_i^\top W_t) g_t + \frac{\partial \alpha_{t,i}}{\partial f_i} \left(\frac{s_t}{\alpha_{t,i}} \right) \quad (\text{S6})$$

Exploiting the derivative of the norm, a straightforward calculation yields

$$\frac{\partial \alpha_{t,i}}{\partial f_i} = -\frac{1}{\|W_t g_t\|_2 \|W_i f_i\|_2^2} \frac{\partial \|W_i f_i\|_2}{\partial f_i} = -\alpha_{t,i} W_i^\top \frac{W_i f_i}{\|W_i f_i\|_2^2}. \quad (\text{S7})$$

Replacing this result in Eq. (S6), gives:

$$\frac{\partial s_t}{\partial f_i} = \alpha_{t,i} \overbrace{W_i^\top W_t}^{\Psi} g_t - s_t \frac{\overbrace{W_i^\top W_i}^{\Psi_i} f_i}{\|W_i f_i\|_2^2}, \quad (\text{S8})$$

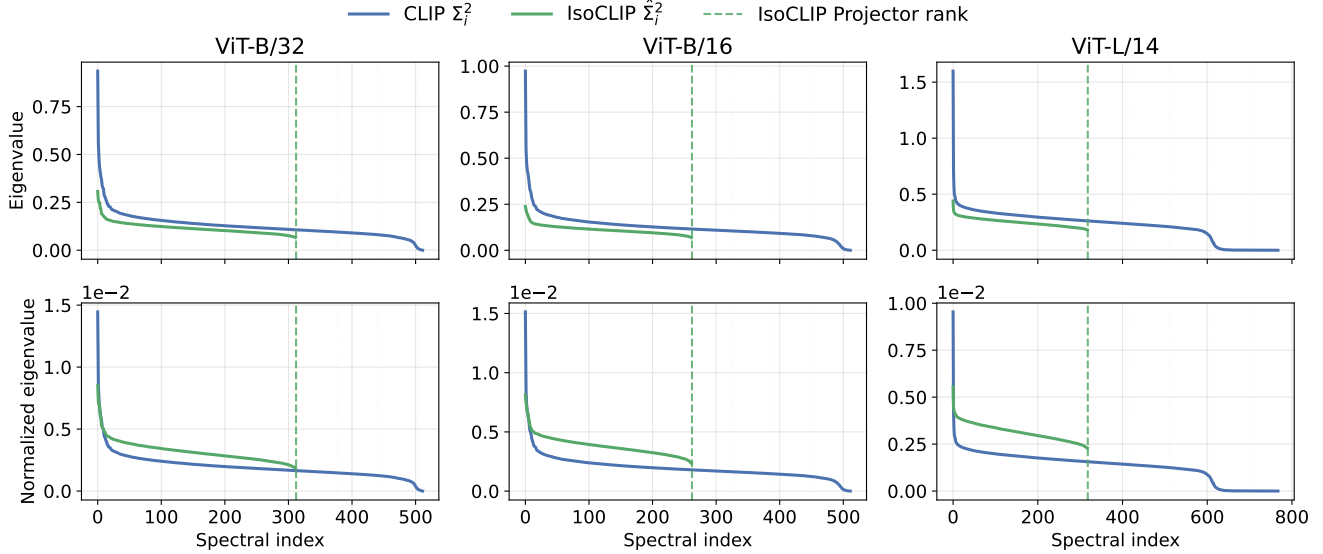


Figure S6. **Spectrum of the intra-modal operator in CLIP (Σ_i^2) and after applying IsoCLIP ($\hat{\Sigma}_i^2$).** (Top) IsoCLIP truncates the spectrum of the intra-modal operator according to the retained subspace defined by the middle-band of the inter-modal operator (Eq. (S9)), resulting in a lower-rank operator. (Bottom) The normalized eigenvalues (obtained by dividing each eigenvalue by the sum of the spectrum) reveal that, after applying IsoCLIP, the intra-modal operator is distributed across more directions than in standard CLIP.

where Ψ and Ψ_i represent respectively the *inter-modal* and *intra-modal* operator, matching the definition in the main paper.

On the role of negative texts. As specified in the main paper and in the previous derivation, we focus on the contribution of the positive text g_t to the gradient (see Eq. (S5)). In general, the full gradient with respect to f_i is obtained by summing over all texts t' in the batch:

$$\frac{\partial \mathcal{L}_{i \rightarrow t}}{\partial f_i} = \frac{1}{\tau} \sum_{t'} (p_{t'} - y_{t'}) \left[\alpha_{t',i} \Psi g_{t'} - s_{t'} \frac{\Psi_i f_i}{\|W_i f_i\|_2^2} \right],$$

where $y_{t'} = 1$ only for the positive text. Negative texts contribute additional image–text directions $g_{t'}$, but they do not introduce new operators: all interactions between image and text features occur through the *inter-modal* operator Ψ , while Ψ_i acts solely as the *intra-modal* normalization term enforcing unit-length image embeddings. Thus, negatives only reweight the contributions of these two operators: repulsion from negatives and attraction toward the positive act exclusively through the inter-modal operator Ψ , while Ψ_i remains a normalization term.

B. Improving Intra-Modal Retrieval via IsoCLIP

At the end of Section 4 in the main paper we discussed that projecting the image and text projectors W_i and W_t onto the subspaces corresponding to the approximately isotropic region of the inter-modal operator spectrum Ψ improves intra-modal retrieval performance. The projected weights are defined as:

$$\widehat{W}_i = W_i U_{S_U} U_{S_U}^\top, \quad \widehat{W}_t = W_t V_{S_V} V_{S_V}^\top. \quad (\text{S9})$$

We now provide additional insights into the mechanism responsible for this improvement. Recall that intra-modal similarity between two image features f_i and $f_{\hat{i}}$ is defined as:

$$\text{sim}(f_i, f_{\hat{i}}) = \frac{f_i^\top (W_i^\top W_i) f_{\hat{i}}}{\|W_i f_i\|_2 \|W_i f_{\hat{i}}\|_2} \propto f_i^\top (W_i^\top W_i) f_{\hat{i}}. \quad (\text{S10})$$

Let us consider the singular value decomposition of the image projector $W_i = U_i \Sigma_i V_i^\top$. Substituting into the similarity expression, we obtain:

$$\text{sim}(f_i, f_{\hat{i}}) \propto f_i^\top (V_i \Sigma_i U_i^\top U_i \Sigma_i V_i^\top) f_{\hat{i}} = f_i^\top V_i \Sigma_i^2 V_i^\top f_{\hat{i}}. \quad (\text{S11})$$

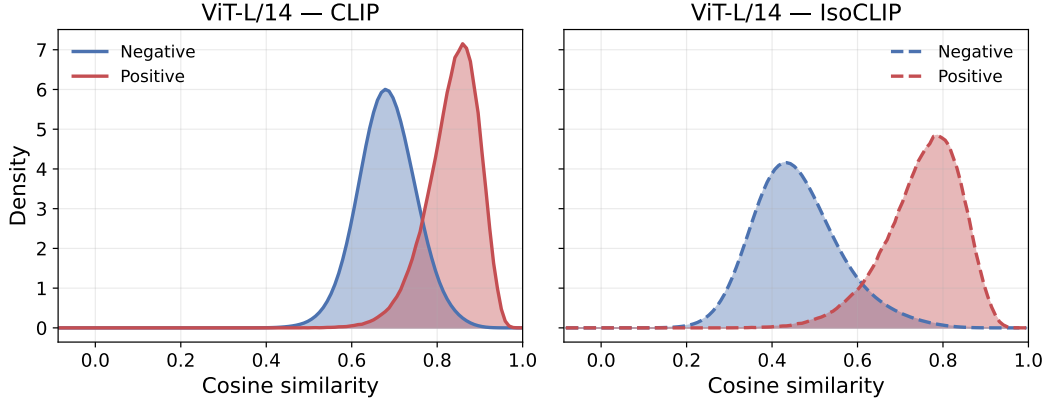


Figure S7. Cosine similarity distribution in image-to-image retrieval for positive and negative pairs on the CUB dataset for CLIP (left) and IsoCLIP (right). Positives are obtained by computing the similarity of each image with all images in the gallery that share the same label, while negatives correspond to the cosine similarity with images having different labels. We observe that the CLIP cosine similarities are concentrated in a narrower range with higher mean values, while IsoCLIP, by weighting more directions in cosine similarity computations, spreads the distribution, shifts the mean similarities to lower values and increases positive and negative separation.

This shows that intra-modal similarity is governed by the intra-modal operator $\Psi_i = W_i^\top W_i = V_i \Sigma_i^2 V_i^\top$. Moreover, this shows that CLIP image-to-image cosine similarity can be interpreted as a weighted summation over the singular directions v_k of W_i , where the weights are given by the squared singular values σ_k^2 . In practice, the spectrum Σ_i^2 is highly anisotropic, so that a small number of singular directions receive excessively large weight in similarity computations. Consequently, similarity scores are dominated by these few directions, reducing the separability between positive and negative pairs.

IsoCLIP mitigates this by restricting the projector to the middle band of the inter-modal spectrum (Eq.S9). The resulting filtered projector \widehat{W}_i can be written as $\widehat{W}_i = \widehat{U}_i \widehat{\Sigma}_i \widehat{V}_i$. The resulting similarity becomes:

$$\text{sim}(f_i, f_i) \propto f_i^\top \widehat{V}_i \widehat{\Sigma}_i^2 \widehat{V}_i^\top f_i. \quad (\text{S12})$$

Because IsoCLIP removes the highly anisotropic top and bottom spectral directions, the spectrum $\widehat{\Sigma}^2$ becomes significantly flatter. As a result, similarity computations distribute weight across a larger number of directions corresponding to the middle band of the inter-modal spectrum, which encode cross-modal semantic alignment.

Fig. S6 visualizes the eigenvalues of the intra-modal operator $W_i^\top W_i$, namely Σ_i^2 for the original CLIP projector and $\widehat{\Sigma}_i^2$ for the IsoCLIP projector, for ViT-B/32, ViT-B/16 and ViT-L/14. The top row shows that IsoCLIP truncates the spectrum according to the retained subspace (Eq. (S9)), resulting in a lower-rank operator. The bottom row shows the normalized spectra with the summation of the eigenvalues. Compared to CLIP, the retained IsoCLIP spectrum is less concentrated in few directions, reducing spectral anisotropy and distributing similarity across a larger set of directions.

IsoCLIP similarity distribution and mAP improvement. It is interesting to observe the effect of the spectra Σ_i^2 and $\widehat{\Sigma}_i^2$ on the cosine similarity distribution. Figure S7 shows the distribution of cosine similarities for positive and negative image pairs using the original CLIP projector (left) and the IsoCLIP projector (right) on CUB images.

In Fig. S7, we observe that the original CLIP projector (left), due to the strong anisotropy, concentrates both the positive and negative cosine similarity distribution in a narrow range (peaks ≈ 0.6 for negative and ≈ 0.9 for positive). This indicates that projected image features occupy a relatively small region of the hyper-sphere.

In contrast, IsoCLIP projects W_i onto the middle-band of the inter-modal operator spectrum, distributing similarity across more directions (Eq. S12). As a result, cosine similarities become less concentrated and shift toward lower values (around ≈ 0.4 for negatives and ≈ 0.8 for positives), indicating that features occupy a larger region of the hypersphere. The reduced overlap between positive and negative similarities (shaded area) leads to higher mAP.

C. Adding Top and Bottom Directions to the Isotropic Middle Band Directions

We complement the experiments in the main paper by incrementally adding top and bottom directions to the 50 middle-band directions shown in Fig. 3 (main paper) on CUB using ViT-B/16. In Fig. S8 we observe that extending the middle band with either top or bottom directions to define the subspace used to project the projector weights in IsoCLIP (Eq. 10 in the

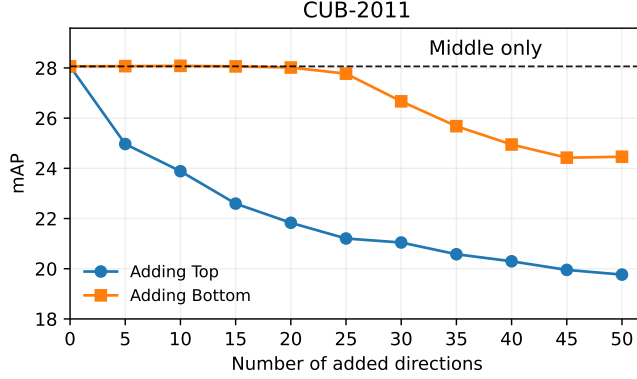


Figure S8. Image-image retrieval mAP performance obtained by iteratively adding top and bottom directions to the 50 middle-band directions when computing IsoCLIP on CUB-2011 dataset using the ViT-B/16.

main paper) degrades mAP retrieval performance, with top directions being more detrimental than bottom ones. This result strengthens the claim that the middle region identified by the inter-modal operator is optimal for improving image-to-image retrieval performance, while the extremes, capturing modality-specific variations, are detrimental.

D. Extension of IsoCLIP to non-linear projection heads

Non-linear projection heads prevent the direct application of IsoCLIP. For instance, models like SigLIP2 [42] employ a Multilayer Perceptron (MLP) head for the image encoder and a linear layer for the text encoder, mapping both modalities into the shared embedding space. We now discuss how to generalize IsoCLIP with non-linear projection heads.

Recent work [47] has shown that linear approximation of Vision Transformer blocks can reveal singular defects in attention feature maps by exploiting data-driven linearization. We propose a simple data-free first-order linearization of the final MLP layer before applying IsoCLIP in models like SigLIP2.

The last MLP visual head of SigLIP2 is defined as:

$$x \leftarrow x + W_2 \phi(W_1 \text{LN}(x) + b_1) + b_2, \quad (\text{S13})$$

where $W_1 \in \mathbb{R}^{m \times n}$, $W_2 \in \mathbb{R}^{n \times m}$ are weight matrices, $b_1 \in \mathbb{R}^m$, $b_2 \in \mathbb{R}^n$ are bias terms and ϕ denotes the GELU activation.

The Layer Normalization (LN) operator is defined as:

$$\text{LN}(x) = \gamma \odot \frac{x - \mu(x)}{\sqrt{\sigma^2(x) + \varepsilon}} + \beta \quad (\text{S14})$$

where γ and β are affine parameters, ε is a small constant, and $\mu(x)$, $\sigma^2(x)$ denote the mean and the variance of x .

Writing $\text{LN}(x) = \gamma \odot \hat{x} + \beta$, the affine parameters can be absorbed into the first linear layer as $\tilde{W}_1 = W_1 \text{Diag}(\gamma)$ and $\tilde{b}_1 = W_1 \beta + b_1$, yielding

$$x \leftarrow x + W_2 \phi(\tilde{W}_1 \hat{x} + \tilde{b}_1) + b_2.$$

Assuming a normalized regime where LayerNorm acts approximately as identity (i.e. $\hat{x} \approx x$), and approximating GELU by its average slope $\phi(z) \approx \frac{1}{2}z$, we obtain the following linearization

$$x \leftarrow \left(I + \frac{1}{2} W_2 \tilde{W}_1 \right) x + \frac{1}{2} W_2 \tilde{b}_1 + b_2. \quad (\text{S15})$$

Accordingly, the effective image projection matrix can be written as

$$W_i = \left[I + \frac{1}{2} W_2 \tilde{W}_1 \quad \frac{1}{2} W_2 \tilde{b}_1 + b_2 \right], \quad (\text{S16})$$

which can be used to apply IsoCLIP as in Eq. S9.

Table S5. Ablation study on the number of OVI pseudo-patches P for text-to-text retrieval on Flickr30K validation set. The highest mAP score for each model is highlighted in bold, with the corresponding value of P used in all experiments.

Backbone	Number of Pseudo-Patches P				
	1	2	4	8	16
ViT-B/16	52.8	52.9	53.1	51.9	50.8
ViT-B/16-open	60.2	59.1	58.0	57.3	57.2

E. Dataset and Implementation Details

In this section, we describe the datasets used and provide implementation details for the modality inversion baselines reported in the tables in the main paper.

E.1. Datasets

For image-to-image retrieval, we consider 13 datasets - ROxford5k [33], RParis6k [33], CUB [45], Stanford Cars [19], Oxford-IIIT Pets [31], Oxford 102 Flowers [29], FGVC Aircraft [24], SUN397 [51], Caltech101 [9], DTD [6], EuroSAT [15], Food101 [4], and UCF101 [41]. We follow the dataset splits proposed in [25] for all datasets. For experiments on ROxford and RParis, we include the R1M distractor set, having about 1 million images, as negative samples for all queries. Here we only report results on the Easy setting from [33]. For the other datasets, we use the training data split as the gallery and the test split as the query set for 12 datasets except CUB where the entire dataset is considered as both the query and gallery.

For text-to-text retrieval, we consider 3 image-captioning datasets - Flickr30k [32], COCO [22], and NoCaps [1]. These datasets contain multiple short captions for each image. Following [25], we consider the first caption of every image as the query and all captions in the dataset as the gallery. The goal is to retrieve the other captions which are associated to the same image. We ignore the images here for the text retrieval task. On an average, COCO and Flickr30K contains 5 captions for each image and the nocaps dataset has 10 captions for each image. We use the captions from the test split for COCO and Flickr30K following the split from [17]. For nocaps, we use the validation set.

We also evaluate image classification on 10 datasets drawn from those used for image retrieval. For this setting, we use the original training splits to compute the class-wise prototypes, and we report performance on the original test splits.

E.2. Implementation Details for Modality Inversion Baselines

We provide implementation details for the Optimization-based Textual Inversion (OTI) and Optimization-based Visual Inversion (OVI) methods used as baselines in our experiments from [25]. These methods map features from one modality to the complementary modality space through iterative optimization.

Optimization-based Textual Inversion (OTI). OTI maps image features to the text embedding space by optimizing a set of pseudo-tokens $v^* = \{v_1^*, \dots, v_R^*\}$ in the token embedding space. Following the original implementation [25], we use a single pseudo-token ($R = 1$) for all backbones, randomly initialized and concatenated with the template sentence "a photo of". We employ the AdamW optimizer with learning rate 0.02, $\beta_1 = 0.9$, $\beta_2 = 0.999$, and weight decay 0.01, performing 150 optimization steps with mixed precision training.

Optimization-based Visual Inversion (OVI). OVI maps text features into the image embedding space by optimizing a set of visual pseudo-patches $w^* = \{w_1^*, \dots, w_P^*\}$ in the patch embedding space. Following the original implementation [25], we adopt the same optimizer settings as OTI, but we run 1000 optimization steps.

Unlike OTI, the optimal number of pseudo-patches P for OVI depends on the model architecture. Following the procedure described in [25], we validated the pseudo patches $P \in \{1, 2, 4, 8, 16\}$ on text-to-text retrieval on Flickr30k validation set, for both ViT-B/16 and ViT-B/16-open, which we introduce in this paper. Table S5 reports the results of this ablation study. For OpenAI ViT-B/16, the best performance is obtained with $P = 4$ pseudo-patches (53.1% mAP). For OpenCLIP ViT-B/16, a single pseudo-patch ($P = 1$) is sufficient, achieving 60.2% mAP.

F. Additional Results and Ablations

In this section, we provide additional results and ablations that complement those in the main paper.

Table S6. **Image-to-image retrieval** performance using *OpenCLIP* ViT-B/32, pre-trained on DataComp dataset, EVA-02 B/16, pretrained on Merged-2B [8] and SigLIP2 B/16 pre-trained on WebLI [42].

Method	Intra-modal	Backbone	Caltech	CUB	ROxford	RParis	Cars	Pets	Flowers	Aircraft	DTD	EuroSAT	Food101	SUN397	UCF101	Avg
Image-Image	✓	ViT-B/32-open	82.3	32.1	50.8	74.7	46.7	44.1	77.0	19.6	36.9	56.4	39.6	36.2	45.7	49.4
OTI (I→T)	✗		83.3	34.3	54.4	75.8	50.5	50.5	78.0	20.1	40.9	54.5	42.9	37.8	48.2	51.6
IsoCLIP	✓		83.4	34.2	56.8	75.8	49.9	47.8	78.2	19.8	37.6	57.7	41.5	36.6	46.3	51.2
Image-Image	✓	EVA-02 B/16	86.9	55.9	52.1	78.3	49.4	55.4	91.5	24.9	35.8	61.2	55.5	41.1	57.0	57.3
IsoCLIP	✓		89.7	58.3	53.0	80.4	55.2	62.8	92.7	25.7	40.0	62.3	57.5	42.2	57.9	59.8
Image-Image	✓	SigLIP2 B/16	89.2	38.1	53.2	76.5	70.8	56.6	89.3	41.8	39.0	50.8	59.2	43.6	59.2	59.0
IsoCLIP	✓		93.1	41.4	54.2	77.9	74.5	64.0	87.2	40.9	43.8	53.2	63.6	46.9	61.8	61.7

F.1. Image-to-Image Retrieval on ViT-B/32-open, EVA-02 B/16 and SigLIP2 B/16

In Tab. S6, we compare IsoCLIP against standard image-to-image retrieval (Image-Image) using only the vision encoder ViT-B/32-open pretrained on the DataComp dataset, as well as against the textual inversion-based approach (OTI). Consistent with the results in the main paper, where ViT-B/16-open with the same pre-training was used, IsoCLIP performs significantly better than Image-Image across all datasets, and achieves slightly lower performance than OTI while requiring substantially lower query latency.

We also evaluate IsoCLIP on EVA-02 B/16 pre-trained on the Merged-2B dataset, where it consistently outperforms standard image-to-image retrieval. Finally, we evaluate SigLIP2 B/16 pre-trained on WebLI, and observe that, despite the linearization of the last MLP projection head (Sec. D), IsoCLIP significantly improves performance on most datasets.

F.2. Image Classification on ViT-B/16-open

Table S7. **Image classification** performance using OpenCLIP ViT-B/16, pre-trained on DataComp dataset, on 10 datasets. We compare IsoCLIP with intra-modal NCM classification and zero-shot classification.

Method	Intra-modal	Classifier	Backbone	Caltech	Cars	Pets	Flowers	Aircraft	DTD	EuroSAT	Food101	SUN397	UCF101	Average
Image-Text	✗	Zero-Shot		96.9	89.8	92.8	75.3	29.8	58.3	53.4	87.5	69.8	67.8	72.1
Image-Image	✓	NCM	ViT-B/16-open	96.7	90.6	88.9	98.6	54.0	74.5	84.4	86.7	74.9	79.9	82.9
IsoCLIP	✓	NCM		97.2	91.4	90.6	98.8	54.5	75.9	85.5	87.1	74.3	80.9	83.6

We extend the experiments on image prototype-based classification with the Nearest Class Mean (NCM) classifier, presented in the main paper, by also evaluating IsoCLIP on ViT-B/16-open. For this model, we observe that IsoCLIP slightly outperforms standard NCM on the image encoder on average and provides consistent improvements on most datasets.

F.3. Comparison with Unimodal DINOv2 B/14

We performed a preliminary comparison with DINOv2 B/14 for image-to-image retrieval. The results are highly dataset dependent: DINOv2 achieves 67.0 mAP on CUB (vs. 53.0 for IsoCLIP PE-Core-B/16), but only 22.3 mAP on Cars, far below IsoCLIP PE-Core-B/16 (62.3 mAP), despite ViT-B/14 processing more image patches due to its smaller patch size. These results suggest that CLIP-style models remain competitive for image-to-image retrieval and highlight the utility of IsoCLIP. A more systematic comparison with self-supervised models is left for future work.

F.4. Experiments on Places365 and iNaturalist

We evaluate IsoCLIP on more benchmarks like Places365 [57] and iNaturalist [44] and present the results in Tab. S8 using PE-Core B/16, SigLIP2 B/16 and EVA-02 B/16. We consider the validation set of Places365 having 35k images and iNaturalist 2021 mini-train version having 500k images for both gallery and query images. The values of k_t and k_b are selected using Caltech101. We show that IsoCLIP consistently improves accuracy on both datasets across different models. On average, IsoCLIP improves by 1.89% on PE-Core B/16, 1.24% on SigLIP2 B/16 and 0.83% on EVA02 B/16.

Table S8. Experiments on Places365 & iNaturalist.

Method	Backbone	Places365	iNat	Avg
Image-Image	PE-Core B/16	16.72	9.61	13.17
IsoCLIP		17.04	13.07	15.06
Image-Image	SigLIP2 B/16	16.17	7.56	11.87
IsoCLIP		17.78	8.43	13.11
Image-Image	EVA-02 B/16	14.54	10.03	12.29
IsoCLIP		15.01	11.23	13.12

F.5. Additional Ablations

Table S9. We compare IsoCLIP against using pre-projection image features for retrieval (Image-Image [Pre]) and against whitening the CLIP image projection weights (W_i^{white}), using ViT-B32 OpenAI and Open ViT-B32 and ViT-B16 pre-trained on Datacomp dataset.

Method	Backbone	Caltech	CUB	ROxford	RParis	Cars	Pets	Flowers	Aircraft	DTD	EuroSAT	Food101	SUN397	UCF101	Average
Image-Image		77.1	22.9	42.6	67.9	24.6	30.5	62.0	<u>14.5</u>	28.1	47.9	32.3	34.3	47.1	40.9
Image-Image [Pre]	ViT-B/32	78.3	23.3	44.9	70.5	24.5	32.7	63.4	14.4	<u>29.5</u>	<u>50.8</u>	<u>34.2</u>	<u>36.0</u>	<u>49.7</u>	42.5
W_i^{white}		<u>78.4</u>	<u>24.5</u>	<u>45.0</u>	<u>70.7</u>	<u>25.9</u>	<u>33.2</u>	<u>63.7</u>	14.3	29.4	50.3	<u>34.2</u>	35.1	48.9	<u>42.6</u>
IsoCLIP		80.8	27.0	47.2	73.8	30.0	40.8	66.5	14.9	<u>30.9</u>	51.5	38.0	36.4	<u>48.4</u>	45.1
Image-Image		82.3	32.1	50.8	<u>74.7</u>	46.7	44.1	77.0	<u>19.6</u>	36.9	56.4	39.6	36.2	45.7	49.4
Image-Image [Pre]	ViT-B/32-open	83.6	31.6	<u>52.8</u>	73.9	46.1	44.6	76.5	19.5	<u>37.3</u>	<u>57.5</u>	<u>39.9</u>	36.9	46.9	<u>49.8</u>
W_i^{white}		83.2	<u>32.9</u>	52.2	74.1	45.6	45.7	77.0	18.7	<u>37.3</u>	57.7	39.8	<u>35.4</u>	46.0	49.7
IsoCLIP		<u>83.4</u>	34.2	56.8	75.8	49.9	47.8	78.2	19.8	37.6	57.7	41.5	<u>36.6</u>	<u>46.3</u>	51.2
Image-Image		85.7	42.8	65.3	83.2	55.8	50.4	<u>84.6</u>	23.1	39.9	57.8	51.1	39.5	52.9	56.3
Image-Image [Pre]	ViT-B/16-open	86.3	42.2	<u>66.9</u>	83.1	56.1	52.4	84.0	<u>23.2</u>	39.9	58.0	52.4	40.9	54.1	<u>56.9</u>
W_i^{white}		86.4	43.8	64.5	83.5	56.2	54.0	84.4	22.4	<u>40.2</u>	<u>58.1</u>	<u>52.8</u>	39.8	53.3	<u>56.9</u>
IsoCLIP		87.6	45.9	67.3	85.0	60.7	57.8	85.8	23.5	42.5	58.6	54.7	39.3	<u>53.4</u>	58.6

We provide additional ablations complementing those in the main paper, using ViT-B/32 OpenAI, Open ViT-B/32, and Open ViT-B/16 models pre-trained on the DataComp dataset. As in the main paper, we compare IsoCLIP against using the *raw pre-projection features* f_i (Image-Image [Pre]) and against applying whitening to the image projector weights (W_i^{white}).

In Tab. S9, we observe that, in general, IsoCLIP outperforms all other approaches across most datasets. Consistent with the results reported in the main paper, IsoCLIP achieves larger gains than both alternatives on the majority of benchmarks. However, when using the models pre-trained on DataComp (ViT-B/32-open and ViT-B/16-open), IsoCLIP attains performance comparable to Image-Image and other baselines on SUN397 and UCF101.

G. Analysis of Hyperparameter Selection

All results reported in Tab. 1 and Tab. 2 of the main paper use the same procedure for selecting the top k_t and bottom k_b singular directions that define the middle-spectrum band used to align the projectors.

Selection of k_t and k_b . As described in the main paper, we select (k_t, k_b) using *Caltech101*, a generic object recognition dataset, for image-to-image retrieval and *COCO* for text-to-text retrieval, and apply these values to *all* the backbones. Table S10 reports the selected values for each model. These hyperparameters differ across backbones because the shape and dimensionality of the singular spectrum of the inter-modal operator depend on the embedding dimensionality and the pre-training dataset, consistent with our analysis of the isotropic middle region in Fig. 2 of the main paper.

For ViT-B/16, the selected values for image-to-image retrieval are $k_t = 200$ and $k_b = 50$, validated on Caltech101 (see Figure 5 left in the main paper).

Table S10. Selection of k_t and k_b for image-to-image and text-to-text retrieval using IsoCLIP. For image classification tasks, we use the same values selected for image-to-image retrieval.

Task	Backbone	k_t	k_b
Image-Image	ViT-B/32	150	50
	ViT-B/32-open	50	50
	ViT-B/16	200	50
	ViT-L/14	250	200
	ViT-B/16-open	100	100
	EVA-02 B/16	150	0
	PE-Core-B-16	300	50
SigLIP2 B/16	350	50	
Text-Text	ViT-B/32	20	100
	ViT-B/16	10	50
	ViT-L/14	10	300
	ViT-B/16-open	2	150

Figure S10 shows that, although these values are not necessarily optimal for every dataset, they generalize well and consistently yield strong performance across all datasets. These plots also indicate that dataset-specific tuning of (k_t, k_b) could further improve performance for some datasets if desired. A similar behavior is observed for text-to-text retrieval in Fig. S9, where varying (k_t, k_b) produces similar trends across datasets.

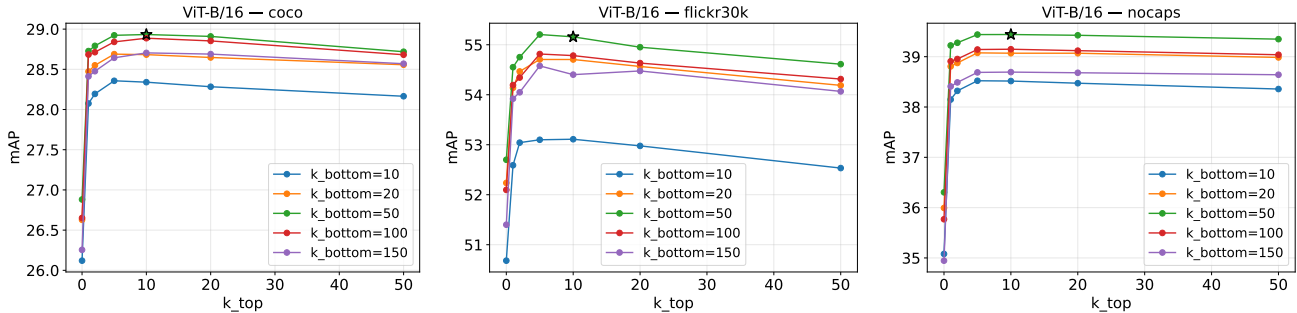


Figure S9. Analysis showing the impact of varying k_t and k_b for the middle band selection across datasets for text-to-text retrieval. The values used in our reported results based on selection from COCO are denoted with stars.

H. Inter-modal Degradation after Applying IsoCLIP

We empirically observe that replacing CLIP projectors with IsoCLIP ones (Eq. S9) reduces CLIP performance on inter-modal tasks such as text-to-image retrieval. This is expected, since the inter-modal operator used to compute inter-modal similarities is explicitly optimized during CLIP training for this purpose, making the original projectors optimal for inter-modal tasks. However, because IsoCLIP modifies only the projector weights, it remains computationally efficient.

In practical settings where a single image gallery is used for both text-image and image-image retrieval, one can store the pre-projection embeddings in the gallery and use the original CLIP projectors for inter-modal similarity while applying IsoCLIP projectors for intra-modal similarity. This introduces only minimal overhead compared to standard zero-shot CLIP inference, since it requires only an additional matrix multiplication with the projection weights.

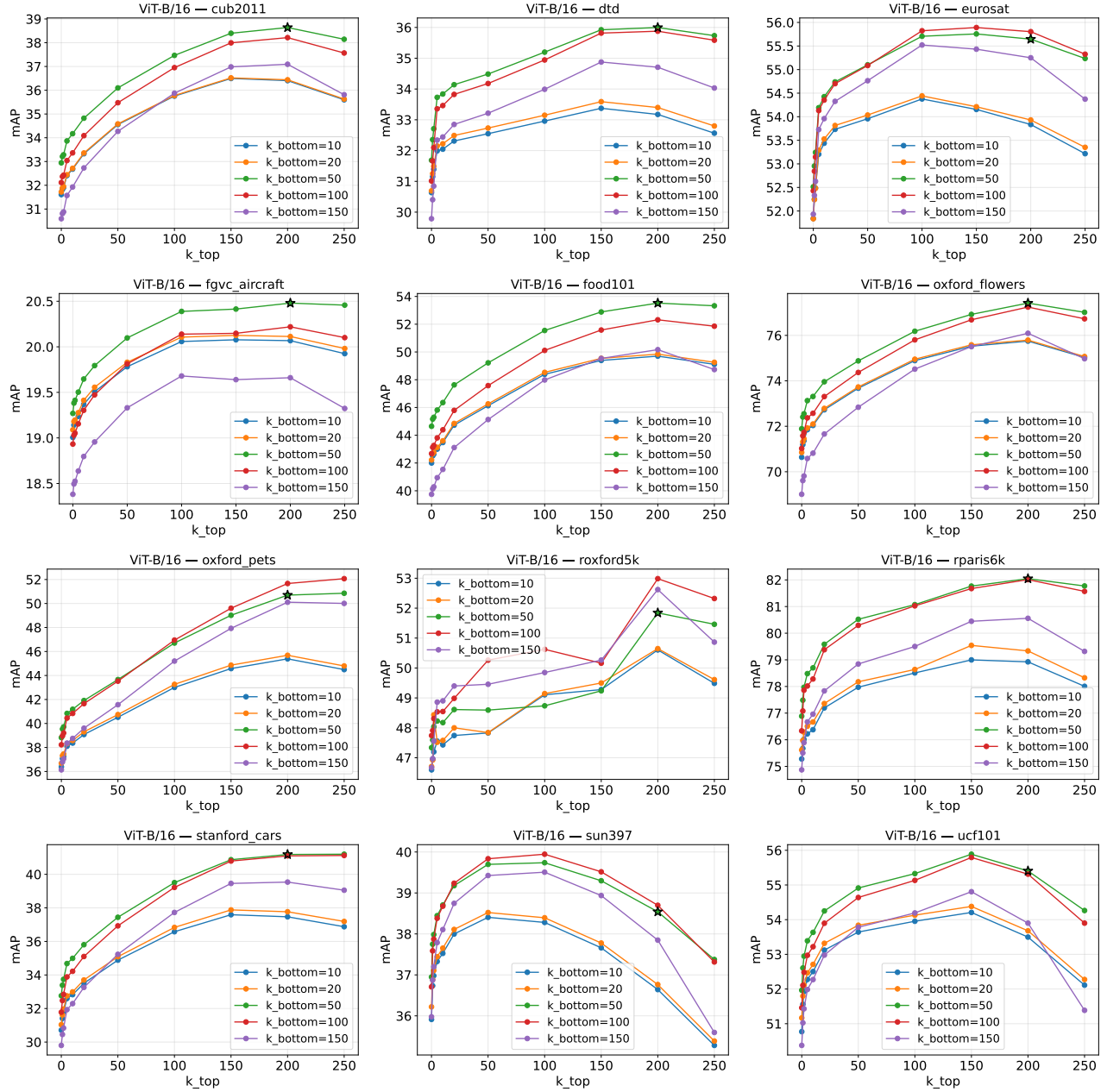


Figure S10. Analysis showing the impact of varying k_t and k_b for the middle band selection across datasets for image-to-image retrieval. The values used in our reported results based on selection from Caltech101 are denoted with stars.

I. The IsoCLIP Algorithm

In this section we provide the complete pseudocode for applying IsoCLIP to pre-trained CLIP models for intra-modal retrieval tasks. The method consists of a one-time preprocessing step that decomposes and aligns the projector weights with the isotropic subspace, followed by the actual retrieval procedure.

Algorithm 1 IsoCLIP Projector Alignment (Training-Free)

Require: Pre-trained CLIP projectors $W_i \in \mathbb{R}^{d \times d_i}$, $W_t \in \mathbb{R}^{d \times d_t}$

Require: Hyperparameters: k_t (top directions to remove), k_b (bottom directions to remove)

Ensure: Aligned projectors $\widehat{W}_i, \widehat{W}_t$

```

1: // Step 1: Construct inter-modal operator
2:  $\Psi \leftarrow W_i^\top W_t \in \mathbb{R}^{d_i \times d_t}$ 
3:
4: // Step 2: Singular Value Decomposition
5:  $U, \Sigma, V^\top \leftarrow \text{SVD}(\Psi)$  ▷  $U \in \mathbb{R}^{d_i \times r}$  (image-side),  $V \in \mathbb{R}^{d_t \times r}$  (text-side),  $\Sigma \in \mathbb{R}^{r \times r}$ 
6:
7: // Step 3: Select middle-band isotropic subspace
8: Identify the subspace  $\mathcal{S}_U = \text{span}\{u_j \mid j \in [k_t, r - k_b]\}$  ▷ Image subspace
9:  $U_{\mathcal{S}_U} \leftarrow [u_{k_t}, u_{k_t+1}, \dots, u_{r-k_b}]$  ▷ Extract columns from  $U$ 
10:
11: Identify the subspace  $\mathcal{S}_V = \text{span}\{v_j \mid j \in [k_t, r - k_b]\}$  ▷ Text subspace
12:  $V_{\mathcal{S}_V} \leftarrow [v_{k_t}, v_{k_t+1}, \dots, v_{r-k_b}]$  ▷ Extract columns from  $V$ 
13:
14: // Step 4: Align projectors to the isotropic subspace
15:  $\widehat{W}_i \leftarrow W_i U_{\mathcal{S}_U} U_{\mathcal{S}_U}^\top$  ▷ Project image projector
16:  $\widehat{W}_t \leftarrow W_t V_{\mathcal{S}_V} V_{\mathcal{S}_V}^\top$  ▷ Project text projector
17:
18: return  $\widehat{W}_i, \widehat{W}_t$ 

```

Algorithm 2 IsoCLIP for Image-to-Image Retrieval

Require: Aligned image projector \widehat{W}_i (from Algorithm 1)

Require: Image encoder $f_\theta(\cdot)$

Require: Query image i_q

Require: Projected gallery features $\{\widehat{F}_{i_1}, \widehat{F}_{i_2}, \dots, \widehat{F}_{i_N}\}$ where $\widehat{F}_{i_n} = \widehat{W}_i f_\theta(i_n)$

Ensure: Ranked list of gallery images

```

1: // Step 1: Extract and project query feature
2:  $f_{i_q} \leftarrow f_\theta(i_q)$  ▷ Extract pre-projection query feature  $\in \mathbb{R}^{d_i}$ 
3:  $\widehat{F}_{i_q} \leftarrow \widehat{W}_i f_{i_q}$  ▷ Project to aligned subspace  $\in \mathbb{R}^d$ 
4:
5: // Step 2: Compute cosine similarities with pre-computed gallery
6: for  $n = 1$  to  $N$  do
7:    $s_n \leftarrow \frac{\widehat{F}_{i_q}^\top \widehat{F}_{i_n}}{\|\widehat{F}_{i_q}\|_2 \|\widehat{F}_{i_n}\|_2}$  ▷ IsoCLIP similarity
8: end for
9:
10: // Step 3: Rank by similarity
11: return Gallery images ranked by  $\{s_1, s_2, \dots, s_N\}$  in descending order

```

Algorithm 3 IsoCLIP for Text-to-Text Retrieval

Require: Aligned text projector \widehat{W}_t (from Algorithm 1)

Require: Text encoder $g_\phi(\cdot)$

Require: Query text t_q

Require: Projected gallery features $\{\widehat{G}_{t_1}, \widehat{G}_{t_2}, \dots, \widehat{G}_{t_M}\}$ where $\widehat{G}_{t_m} = \widehat{W}_t g_\phi(t_m)$

Ensure: Ranked list of gallery texts

1: **// Step 1: Extract and project query feature**

2: $g_{t_q} \leftarrow g_\phi(t_q)$

▷ Extract pre-projection query feature $\in \mathbb{R}^{d_t}$

3: $\widehat{G}_{t_q} \leftarrow \widehat{W}_t g_{t_q}$

▷ Project to aligned subspace $\in \mathbb{R}^d$

4:

5: **// Step 2: Compute cosine similarities with pre-computed gallery**

6: **for** $m = 1$ to M **do**

7: $s_m \leftarrow \frac{\widehat{G}_{t_q}^\top \widehat{G}_{t_m}}{\|\widehat{G}_{t_q}\|_2 \|\widehat{G}_{t_m}\|_2}$

▷ IsoCLIP similarity

8: **end for**

9:

10: **// Step 3: Rank by similarity**

11: **return** Gallery texts ranked by $\{s_1, s_2, \dots, s_M\}$ in descending order
